

Double Higgs Production at the Linear Colliders and the Probing of the Higgs Self-Coupling

F. Boudjema¹ and E. Chopin²

*Laboratoire de Physique Théorique ENSLAPP **
B.P.110, 74941 Annecy-Le-Vieux Cedex, France

1. E-mail:BOUDJEMA@LAPPHP8.IN2P3.FR

2. E-mail:CHOPIN@LAPPHP8.IN2P3.FR

Abstract

We study double Higgs production in the e^+e^- and $\gamma\gamma$ modes of the linear collider. It is also shown how one can probe the scalar potential in these reactions. We discuss the effective longitudinal W approximation in $\gamma\gamma$ processes and the $W_L W_L$ luminosities in the two modes of a high-energy linear collider. A generalised non-linear gauge-fixing condition, which is particularly useful for tree-level calculations of electroweak processes for the laser induced collider, is presented. Its connection with the background-field approach to gauge fixing is given.

ENSLAPP-A-534/95
hep-ph/9507396
July 1995

* URA 14-36 du CNRS, associée à l'E.N.S de Lyon et à l'Université de Savoie.

1 Introduction

Now that there has been striking direct evidence for the top quark [1] with a mass that fits neatly with what one deduces from the precision measurements at LEP1 and SLC, the matter content of the Standard Model, \mathcal{SM} , is complete. What is still desperately missing is the scalar particle of the model, the Higgs. Intimately related to the existence of this cornerstone particle is the mechanism of symmetry breaking. The elucidation of its realisation will most probably have to await the next generation of high energy colliders. Once the Higgs has been discovered it will be essential to scrutinize all its properties, like its couplings to the other particles and its parity. These will be precision measurements that are best conducted in a clean environment and therefore one hopes to conduct these tests at the next linear collider in its e^+e^- mode as well as the much discussed $\gamma\gamma$ mode[2]. Among these tests one should include the probing of the self-couplings of the Higgs. These self-couplings have undeservedly received very little attention[3, 4, 5] and yet, in the \mathcal{SM} , they directly emerge from the pure non-gauge Higgs-Goldstone potential that realises the symmetry breaking. Let us recall that with the assumption of one Higgs doublet Φ , which most naturally implements the well confirmed $\rho = 1$, and in order that spontaneous symmetry breaking ensues with the correct value of the vacuum expectation value that gives the gauge boson masses, the most general potential has the form

$$V_{SSB} = -\mathcal{L}_{SSB} = \lambda \left\{ \left[\Phi^\dagger \Phi - \frac{v^2}{2} \right]^2 + \sum_{n \geq 3} \frac{\kappa_n}{\Lambda^{2(n-2)}} \left[\Phi^\dagger \Phi - \frac{v^2}{2} \right]^n \right\} \quad (1.1)$$

Only the first term, of dimension four, is needed in the \mathcal{SM} to trigger symmetry breaking and to ensure renormalisability. This term introduces the one scale that feeds the masses for all the particles in the SM, $v = 246 GeV$. It is also characterised by the parameter λ whose presence has not been established, let alone measured since this extra parameter is directly related to the Higgs mass and measures its self-couplings as well as its coupling with the would be longitudinal weak bosons. These self-couplings are large when the Higgs mass is large. With the minimal prescription the tri-linear and quadri-linear Higgs self-couplings will be directly deduced when the Higgs mass is known.

The higher order terms necessarily parameterise the most general scalar potential and could indicate a non-standard Higgs, possibly a bound state that evades the naturalness argument without invoking supersymmetry. These “beyond-the- \mathcal{SM} ” terms introduce a new scale Λ , in a sense a new “curvature”, that may have nothing to do with the Fermi scale, *i.e.* v . This new potential changes the tri-linear and quadri-linear couplings. Since these new couplings involve neither the matter particles nor the gauge particles a direct unambiguous litmus test for their existence is only possible through multiple Higgs pro-

duction. Since one expects these multiparticle cross sections to be small one should look for these signatures in an environment where one is not swamped by a large background and where there is the least theoretical uncertainty in the standard model calculation, thus high energy e^+e^- machines seem to be the ideal place to study these reactions.

e^+e^- operating in the TeV range are being very seriously considered. These also offer the possibility of running not only in the “classic” e^+e^- mode but can also be turned into $\gamma\gamma$ or $e\gamma$ colliders by converting the electron into a highly energetic photon through Compton backscattering with the help of a laser[2]. Recently there has been an intense activity in the physics that can be investigated at these new types of colliders and a research and development programme is in full swing.

The aim of this paper is three-fold. First, we want to give the expected cross sections for double Higgs production at TeV energies at the e^+e^- colliders. In so doing we will present the details of the first calculation of the process $\gamma\gamma \rightarrow W^+W^-HH$ and derive an approximate analytical expression for its high-energy behaviour through the use of the structure function approach, in this case the W content of the photon. We will then compare the effective luminosity for W_LW_L in the e^+e^- and the $\gamma\gamma$ modes. Another purpose is to put forth the suggestion that for processes with multi- W 's especially in association with photons it is by far advantageous to calculate in a non-linear gauge[6]. Till now these type of gauges have been used for loop calculations, we will show how they can ease the calculational task in the case of tree-level amplitudes with many gauge bosons. In passing, we will point to the connection between the generalised non-linear gauge that we introduce in this paper and the background field inspired gauges[7] applied to the $SU(2) \times U(1)$ [8] that have been much discussed in the last year[9]. As a third purpose we will discuss how to measure the tri-linear Higgs self-coupling and the limit we could hope to extract at the 2TeV e^+e^- collider in its different modes. We will also investigate and compare with the limits that one may tentatively set on this coupling from indirect measurements.

The paper is organised as follows. In the next section we deal with the process $\gamma\gamma \rightarrow W^+W^-HH$ and show how efficient a suitable gauge fixing condition can be in tremendously easing the computational task. We study various distributions and comment on the effect of polarisation, both initial and final. Section 3 compares different processes for double Higgs production at the e^+e^- and the $\gamma\gamma$ modes including the effect of photon spectra. This comparison and the discussion in section 2 lead us, in section 4,

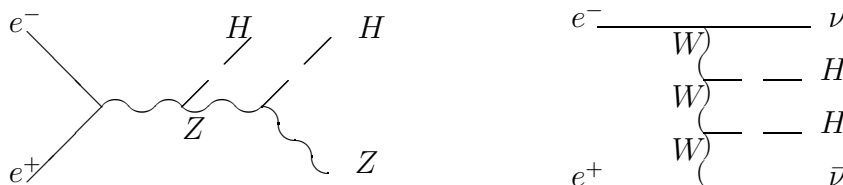
to inquire about the validity of the effective W approximation both for e^+e^- [10] and $\gamma\gamma$ reactions [11, 12], in other words finding approximations by considering the longitudinal W as a parton. Especially interesting is the longitudinal W content of the photon. We study both the case of a heavy Higgs and a light Higgs. When referring to a heavy Higgs we have in mind a Higgs that decays into the weak vector bosons and that is predominantly coupled to their longitudinal parts. Our representative example of a heavy Higgs throughout the paper will be $M_H = 400\text{GeV}$. As a by-product we give the full helicity amplitudes for the hard sub-process $W^+W^- \rightarrow HH$ including the anomalous H^3 coupling. In section 5 we show how we can test for the presence of a tri-linear Higgs coupling and give the limit one may hope to set on its strength at a 2TeV e^+e^- machine and comment on the improvement that a higher energy collider can bring. We conclude in section 6. In an Appendix we discuss in detail the “generalised” non-linear gauge fixing condition, show how the background field gauge-fixing condition can lead to a special case of the non-linear constraint. Full Feynman rules, including the ghosts, are presented for general values of the non-linear gauge parameters.

2 $\gamma\gamma \rightarrow W^+W^-HH$

2.1 Motivation

Double Higgs production in the classic mode of the e^+e^- has been considered sometime ago[3, 13, 14]. As with the case of single H production one has two different mechanisms obtained by grafting another Higgs to the single Higgs production mechanism: either as a double Higgs bremsstrahlung off the Z : $e^+e^- \rightarrow ZHH$ [3, 13] (see Fig. 1) or through WW fusion[14] leading to $e^+e^- \rightarrow \nu_e\bar{\nu}_eHH$ (Fig. 1). A similar mechanism[14] through ZZ fusion ($e^+e^- \rightarrow e^+e^-HH$) gives much smaller cross sections due to the much smaller coupling of the Z to the electron than the W .

Figure 1: *Representative diagrams that contribute to $e^+e^- \rightarrow ZHH$ and $e^+e^- \rightarrow \nu_e\bar{\nu}_eHH$.*

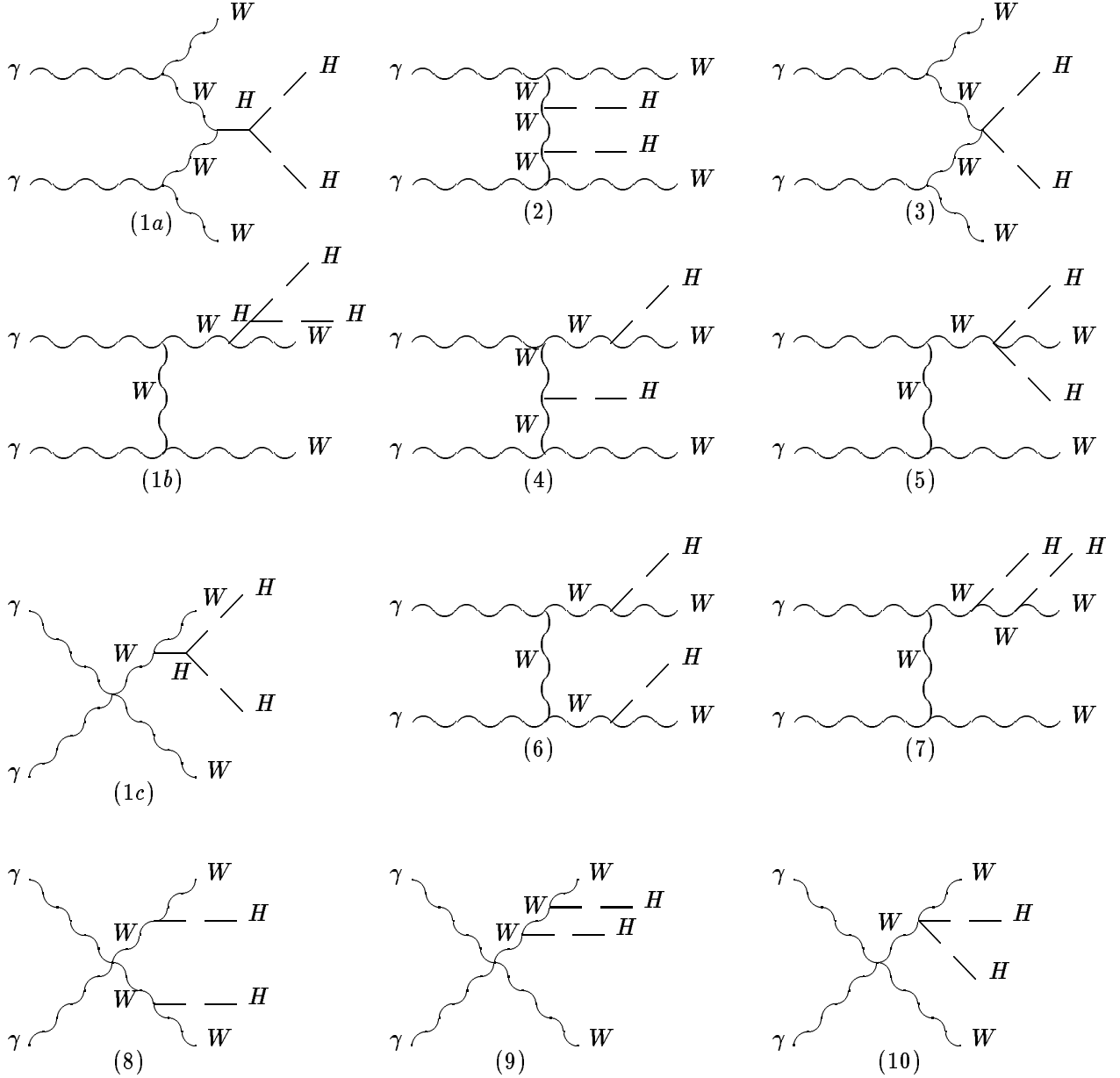


The one-loop induced $e^+e^- \rightarrow HH$ [15] has also been considered and found to be dismal. The interest in $\gamma\gamma \rightarrow W^+W^-HH$ stems from the observation that since the cross section for the basic process $\gamma\gamma \rightarrow W^+W^-$ is really enormous[16] with a value of about 80pb at 400GeV and not decreasing with energy due to the spin-1 t-channel W -exchange, one could use it as a backbone to hook yet more particles, especially the neutrals. This idea has been successfully applied to single Higgs production through $\gamma\gamma \rightarrow W^+W^-H$ [17] where it was found that at high enough energy, where one is not penalised by the reduced phase space, this reaction occurs at a higher rate than its e^+e^- equivalent $e^+e^- \rightarrow \nu_e\bar{\nu}_eH$ [18] which is the dominant mechanism for single Higgs production at e^+e^- . It is then hoped that $\gamma\gamma \rightarrow W^+W^-HH$ can compete with double Higgs production in e^+e^- .

2.2 Non-linear gauge fixing for tree-level $\gamma\gamma$ processes

When switching from e^+e^- to $\gamma\gamma$ production the calculational task becomes much more arduous especially as more gauge particles are involved. Not only does the number of diagrams increase tremendously but each diagram has a much more complicated structure brought about by the handling of the non-Abelian vertices, as well as by the form of the massive propagators in the unitary gauge. For instance, in the case at hand, comparing the $e^+e^- \rightarrow \nu_e\bar{\nu}_eHH$ with $\gamma\gamma \rightarrow W^+W^-HH$, one notices that for the former only four diagrams are present (neglecting justifiably the electron mass) and that we can simply leave out the ‘‘longitudinal part’’ ($k_\mu k_\nu/M_W^2$ parts) of the W propagators, since the W ’s couple to conserved currents. One thus has a simple calculation to perform with compact formulae for the helicity amplitudes. As can be seen from the list of diagrams (Fig. 2) contributing in the unitary gauge to $\gamma\gamma \rightarrow W^+W^-HH$ the situation is much more complex: one has 12 possible graph topologies which upon symmetrisation bring about a total of 46 diagrams. Moreover, beside the non-Abelian vertices one has to keep the ‘‘longitudinal’’ terms which in the case of three W exchanges ‘‘eightuples’’ the number of terms! What is worse for an already complex situation and more dangerous in a numerical implementation of the amplitudes, is the fact that these longitudinals which are associated with the very bad high energy behaviour of the cross section, contribute large numerical factors: $\sim (E_W/M_W)^{2n} \sim (s/M_W^2)^n$, n counting the number of propagators that can be large for multiple vector bosons amplitudes. These factors eventually largely cancel when the full set of diagrams is taken into account. In a numerical implementation of the amplitudes, the instability that these terms might introduce is to be avoided while it is essential to make the calculation as tractable as possible and with expressions that

Figure 2: Different topologies of Feynman diagrams contributing to $\gamma\gamma \rightarrow W^+W^-HH$ in the unitary gauge. Figures (1a), (2) and (3) are the fusion type diagrams. All others can be considered bremsstrahlung. (1a-c) contain the triple Higgs vertex.



can be as compact as possible.

Almost invariably the way out is to revert to the standard 't Hooft-Feynman gauge, thus eliminating the annoying “longitudinal” terms. However, especially with the presence of many W 's there is a price to pay, in that more diagrams containing the compensating Goldstone fields have to be added even though the expressions derived from each diagram are more compact than in the unitary gauge. The best of both worlds would be to keep the same (or sensibly the same) number of diagrams as in the physical gauge and at the same time rendering the expressions much more compact. This is possible if one judiciously chooses a non-linear gauge fixing condition and selects the gauge parameter to correspond to the 't Hooft-Feynman gauge. The main reason, in the non-linear gauges, the Goldstone bosons do not appear in most diagrams is due to the fact that the $W^\pm\varphi^\mp\gamma$ is not present. The underlying principle behind the vanishing of this vertex is that the gauge fixing is such that it still does not explicitly break the $U(1)_{em}$ and as a consequence one should not expect an electromagnetic “particle-changing” current such as $W^\pm\varphi^\mp\gamma$.

The widespread choice of the linear gauge fixing condition [†]

$$\mathcal{L}_{linear}^{Gauge-Fixing} = -\frac{1}{\xi}|\partial_\mu W^{\mu+} + i\xi M_W\varphi^+|^2 \quad (2.2)$$

only eliminates the $W^\pm\varphi^\mp$ mixing, while for a typical non-linear gauge

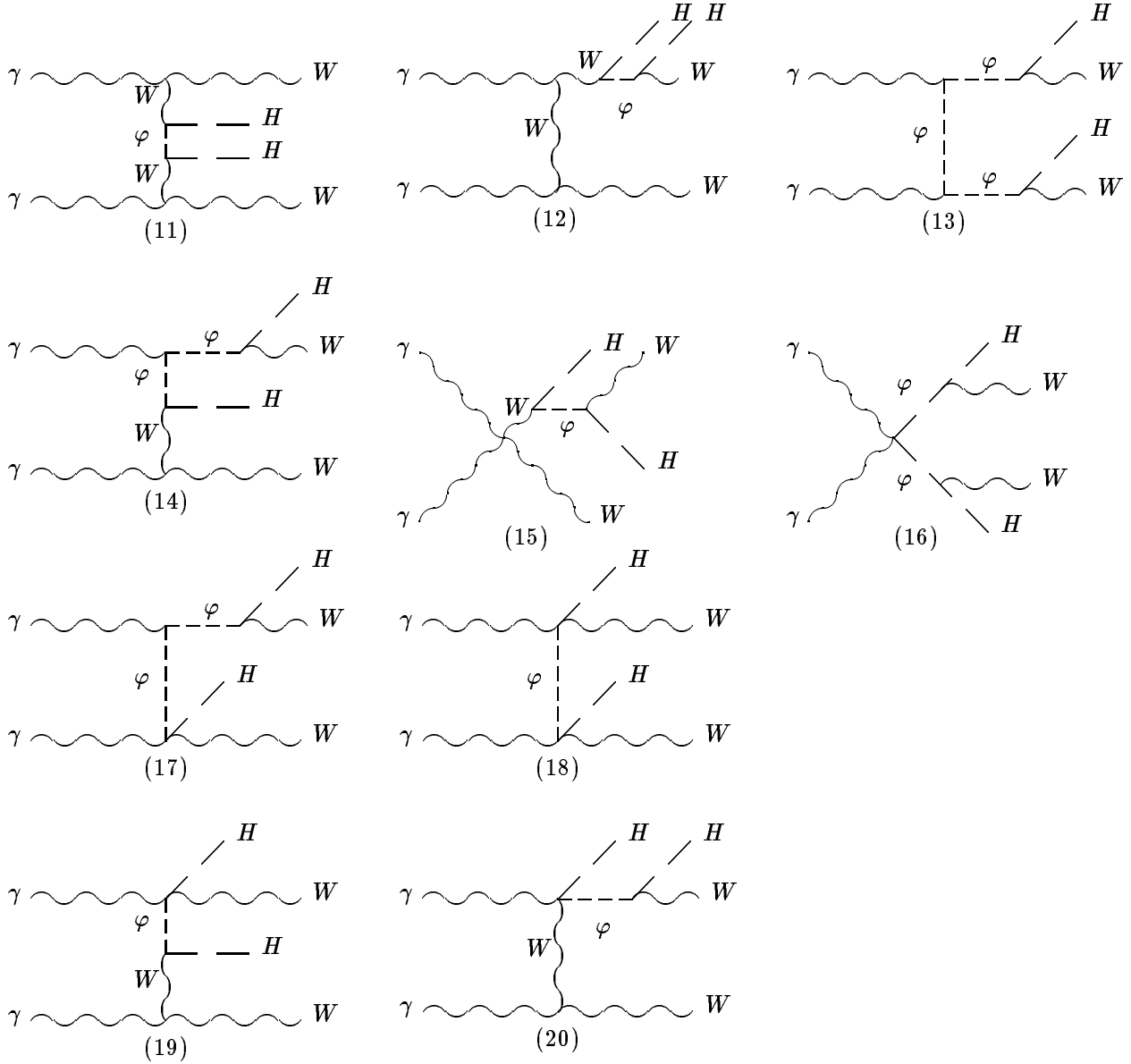
$$\mathcal{L}_{non-linear}^{Gauge-Fixing} = -\frac{1}{\xi}|(\partial_\mu + ieA_\mu + ig\cos\theta_W Z_\mu)W^{\mu+} + i\xi(M_W + \frac{g}{2}H)\varphi^+|^2 \quad (2.3)$$

the $W^\pm\varphi^\mp\gamma$ will disappear due to the use of the covariant derivative with respect to the $U(1)$ current. In fact, with the above choice the covariant derivative is along the full T_3 neutral direction of the $SU(2)$ group. We have already used a slight variation of the above [17, 12] gauge condition for the calculations of $\gamma\gamma \rightarrow W^+W^-Z, W^+W^-\gamma, W^+W^-H$ and have found tremendous simplifications. For those processes the last term involving the Higgs does not enter, however for $\gamma\gamma \rightarrow W^+W^-HH$ it is essential because it eliminates the “unnatural” $W^\pm\varphi^\mp\gamma H$ that may enter at this order (see Fig. 3). The only other application of this gauge-fixing for tree-level amplitudes in the electroweak theory that we are aware of is the recent calculation of $\gamma\gamma \rightarrow W^+W^-W^+W^-, W^+W^-ZZ$ [19].

These are not the only simplifications that the non-linear gauge fixing conditions (with the Feynman parameter $\xi = 1$) bring. Both the tri-linear $W^+W^-\gamma$ and quartic $W^+W^-\gamma\gamma$

[†]Our conventions are defined in the Appendix.

Figure 3: *Some extra topologies of Feynman diagrams that have to be added in a renormalisable gauge even when the $W^\pm\varphi^\mp\gamma$ is absent. The last 4 topologies are cancelled with the gauge-fixing that we take.*



are simplified. The latter now contains only one term out of three, moreover all diagrams containing this coupling trivially vanish when the two incident photons have opposite helicities ($J_Z = \pm 2$). As for the tri-linear coupling (see Appendix) it is most usefully split into a universal “convection” current (present for the case of scalars and fermions) and a spin current that is automatically transverse in the photon. To make full use of these gauges one has to combine them with the calculation of the helicity amplitudes. In fact, recent developments in the calculation of QCD processes[20], especially the so-called string inspired organisation, can be understood as being (partly) based on the exploitation of similar gauges. This type of gauges has an obvious connection and similarity with the so-called background gauges[7] which, within the $SU(2) \times U(1)$ model, have been resurrected in the last year [9]. The underlying idea is the same though: one strives to maintain an explicit gauge covariance (after gauge-fixing) in the classical fields (external fields or external currents). For this one splits the fields into a quantum and a classical part and take the covariant derivative with respect to the classical gauge fields.

The above non-linear gauge can be generalised. For instance, for other applications, one can arrange for the $W^\pm \varphi^\mp Z$ to vanish as well. More generally we can tune the parameters of the following gauge-fixing term for the W 's:

$$\mathcal{L}_{non-linear}^{Gauge-Fixing} = -\xi^{-1} |(\partial_\mu + ie\tilde{\alpha}A_\mu + ig \cos \theta_W \tilde{\beta}Z_\mu)W^{\mu+} + i\xi \frac{g}{2}(v + \tilde{\delta}H - i\tilde{\kappa}\varphi_3)\varphi^+|^2 \quad (2.4)$$

In the Appendix we give the Feynman rules for this most general gauge fixing term and will explicitly spell out the connection with the background gauge applied to $SU(2) \times U(1)$.

2.3 Total cross section, energy dependence and polarisations

With the above choice of gauge it is a relatively easy task to compute the helicity amplitudes. As a check on our calculation we verified that the amplitudes were transverse in the photon momenta. Moreover, since the diagrams that involve the triple Higgs vertex constitute a gauge invariant subset we have also checked that this subset is also transverse in the photons. One way to argue that this subset is gauge invariant is to observe that this is the same subset that constitutes the whole of the $\gamma\gamma \rightarrow W^+W^-H$ amplitude. Therefore, if one “fuses” the two Higgses into a single state one has an effective Higgs and thus one is effectively calculating $\gamma\gamma \rightarrow W^+W^-H$. Another way of seeing this is to observe that the triple Higgs vertex emerges from another part of the Lagrangian (scalar potential) than the WWH (covariant derivative on the Goldstone field). Upon modifying the strength of this vertex, transversality in the photon is still maintained. We will come

back to this point later when discussing the inclusion of a non-standard value for the Higgs and how, again, the non-linear gauge fixing brings a welcome simplification.

Our phenomenological analyses will be mainly for centre-of-mass energies up to 2TeV, *i.e.*, in the range considered for the next generation of linear colliders before including any spectra for the $\gamma\gamma$ luminosity. However, this process having quite interesting features which are more easily revealed at high energies we will also discuss the case of much higher energies and heavy Higgses so as to be able to check whether a description in terms of structure function, W_L inside the photon, can be applicable.

We have taken $\alpha = 1/137$ everywhere with $M_W = 80.2\text{GeV}$ and $\sin^2\theta_W = s_W^2 = 0.2325$. One may question why we decided against the use of $\alpha = 1/128$. For the photon vertex (with an on-shell photon: $q^2 = 0$) this is perfectly justified. Indeed $\gamma\gamma \rightarrow W^+W^-$ has to be calculated with this value of α , this has also been confirmed by computing the one-loop corrections to this reaction[21]. As for the WWH couplings one may choose to use $\alpha = 1/128$ by relating this to G_F . Sticking with the latter choice our numbers have to be scaled by a factor $(137/128)^2$.

The first conclusion is that the cross sections are rather small for the foreseeable colliders. For a Higgs mass of 100GeV and with a total $\gamma\gamma$ centre-of-mass energy of 2TeV, we find a total cross section of about 0.21fb giving some 63 events for an integrated luminosity of $\int \mathcal{L} = 300\text{fb}^{-1}$, before including the various W 's branching ratios and convoluting with the $\gamma\gamma$ luminosity spectra. There is about a factor of α as compared to $\gamma\gamma \rightarrow W^+W^-H$ [17] for the same mass and energy. These events will thus be rare events that would need to be analysed after a long run. On the other hand, as with all rare processes, this cross section is therefore ideal for the investigation of New Physics. In this respect, it is essential to study in detail all the characteristics of this process and its salient signatures.

The behaviour of the cross section reflects a few of the characteristics of the $\gamma\gamma \rightarrow W^+W^-$ process. The t-channel W exchange enhancement, responsible for the constant asymptotic $\gamma\gamma \rightarrow W^+W^-$ cross section, brings for this multiple particle production a logarithmic growth as the energy increases (Fig. 4). Moreover, one still has the dominance of the transverse W 's: each time one replaces a transverse W by a longitudinal one loses an order of magnitude in the total cross section. This recurring feature is well rendered in Fig. 4. As for the photon polarisations, and again as is the case with the $\gamma\gamma \rightarrow W^+W^-$ at high energy, there is very little dependence on the helicity combinations

Figure 4: *Contribution of the different polarisation states of the W's.*

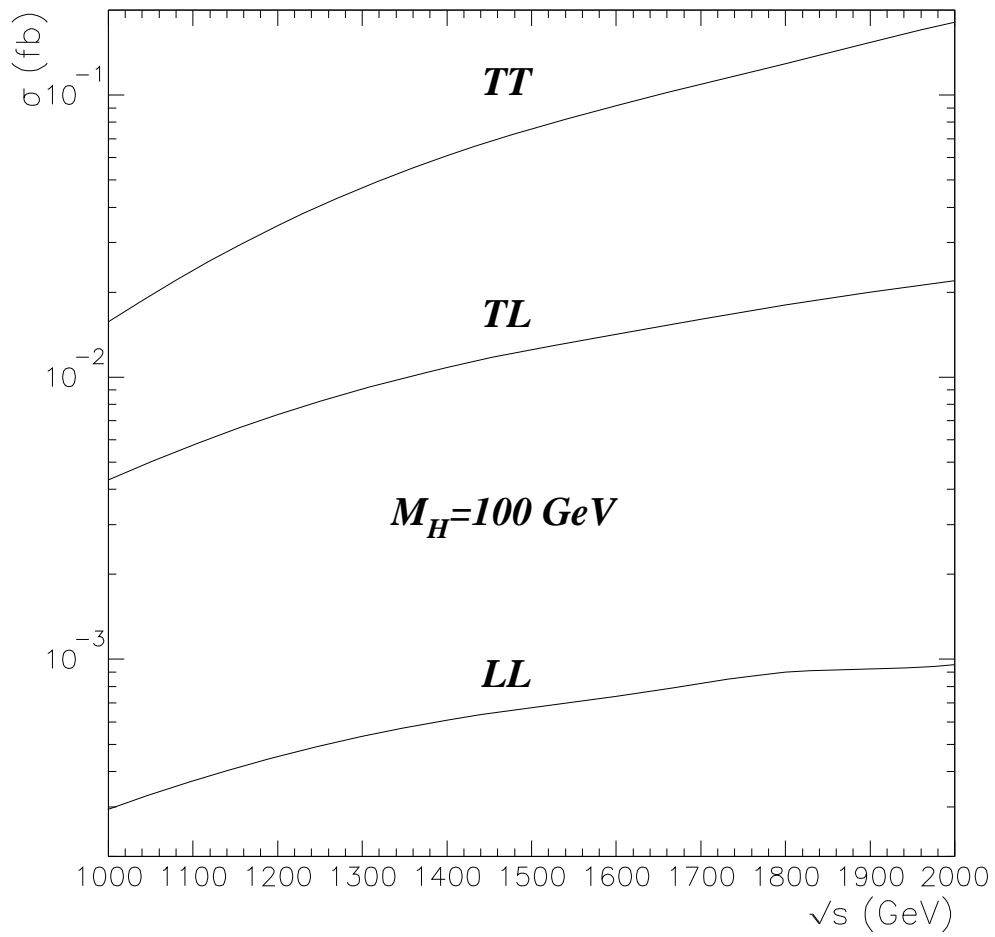
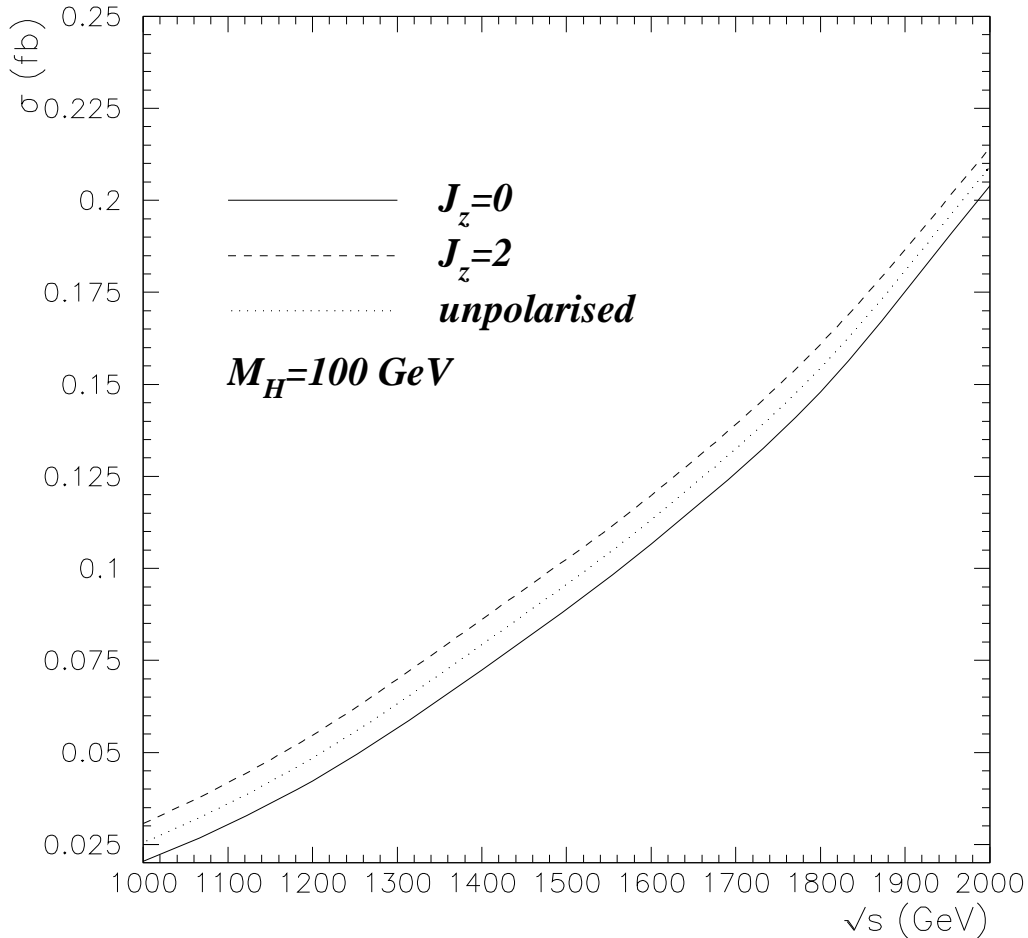


Figure 5: *Contribution of the $J_Z = 0$ and $J_Z = 2$ to the total cross section.*



of the initial photons already at 1TeV. This is clearly seen in Fig. 5. where we note that there is a slight preference for a setting with opposite photon helicities ($J_Z = 2$) that tends to attenuate as the energy increases. This feature persists for a higher Higgs mass.

2.4 Higgs mass dependence

At 2TeV centre-of-mass the cross section drops precipitously with increasing Higgs mass. For instance, for a 200GeV Higgs mass it is twice as small as for 100GeV Higgs with about a tenth of fb. For a 300GeV Higgs there is again another factor 1/2 reduction. In this process that involves the triple Higgs self-coupling the Higgs dependence does not only

enter trivially in the phase space (or to a lesser extent through the propagator) but it should be kept in mind that the Higgs self coupling itself is proportional to square of the Higgs mass. We should thus expect this feature to contribute in, somehow, balancing out the phase space reduction. This however occurs only slightly at much higher energies. The reason is the following: in the minimal \mathcal{SM} the $W_L W_L H H$ is also of enhanced strength (*i.e* proportional to M_H^2/M_W^2) as can be most easily seen by reverting to the equivalence theorem[22] which, here, will tell us that this is $\varphi^\pm \varphi^\mp H H$. The latter stems from the Higgs potential also and has the same strength. The other observation is that for a heavy enough Higgs, the fusion diagrams are important and as we will show below are dominated by the longitudinal quasi-real W 's. Then a destructive interference takes place between the diagrams involving the triple-Higgs vertex in which we are most interested and the ones involving the $W W H H$ vertex. This will become clearer when we study $W^+ W^- \rightarrow H H$. To bring out this important feature in evidence, and having in view the probing of the Higgs self-couplings (Signal) and those where this coupling is absent (Background). As figure 6 shows, at 2TeV there is already substantial destructive interference that is most operative when the Higgs mass is in excess of 350GeV (heavy Higgs mass). At 5TeV one sees clearly that both the ‘‘Signal’’ and ‘‘Background’’ increase with increasing Higgs masses (taking M_H up to $M_H = 700\text{GeV}$), however they conspire to give a much smaller cross section. Note that the outgoing transverse W 's dominate the cross section for all values of M_H when one is far from threshold.

2.5 Distributions

The logarithmic growth of the cross section, in particular for the transverse modes of the W 's, is no surprise. Again this stems from the multiple W exchanges, this feature is also present in single Higgs production[17]. Indeed, the cross section is dominated by the very forward (backward) W 's. This can be seen in the angular distribution of the outgoing W 's. Already at 1TeV (where the cross section is very small) the forward peak is fantastic (See Fig. 7)

For a multiple particle production such as this one there are quite a number of distributions that one may want to study. Knowing these distributions will be most useful for optimising the search for New Physics. We have another motivation for analysing the different distributions: we would like to find out which diagrams are most dominant so that one could work out some approximation for the whole process. First, since we have two Higgses in the final state we have preferred to single them out by labelling them as the

Figure 6: *Higgs mass dependence of the $\gamma\gamma \rightarrow W^+W^-HH$ cross section at 2TeV and 5TeV. The contribution of the diagrams involving the triple Higgs vertex (Signal) and the rest (Background) is shown separately. Also shown is the contribution of the transverse W's (TT). "Total" stands for the contribution summed over all helicities of the W's.*

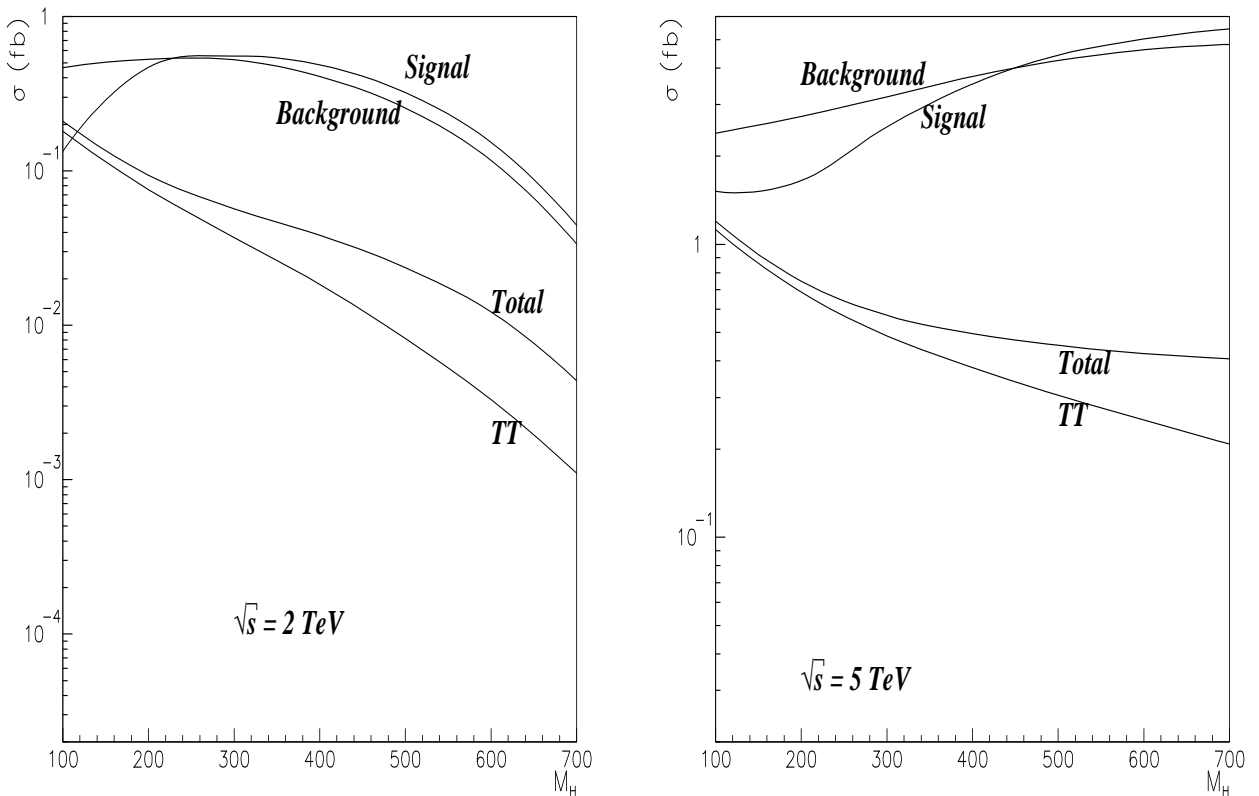
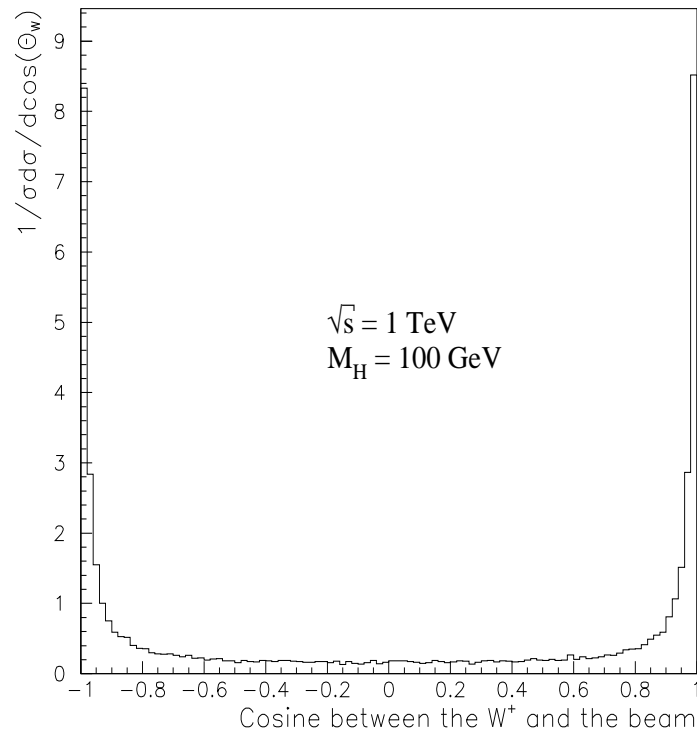


Figure 7: Angular distribution of any W with respect to the beam for $M_H = 100\text{GeV}$ and $\sqrt{s} = 1\text{TeV}$.



least and most energetic Higgs. These two have quite different angular distributions (measured with respect to the beam) especially for the case of a light Higgs ($M_H = 100\text{GeV}$). For the latter, while the most energetic H is preferentially carried along the W direction (that is in the forward/backward), the least energetic has an almost uniform distribution even for very high centre-of-mass energies, Fig. 8. For a heavier Higgs, the two Higgses are both clearly preferentially forward.

As for the energy distributions, we see from Figs. 9 that it is the transverse W that carries on average most of the energy, the much less dominant longitudinal W 's have a rather uniform spectrum. Especially for the light Higgs, one of the two Higgses is almost a bremsstrahlung Higgs that takes along very little momentum Figs 10. This is the case even at very high energies (5TeV) and means that the decay products (the b's) will be clearly separated. In view of the characteristics of the energy and escape angle of the Higgses, that show different behaviour for the light and heavy Higgs, there is in the case of the light Higgs some evidence for the fact that the contribution of Higgses emitted as bremsstrahlung off the external W 's is not negligible. This is because the least energetic Higgs carries little energy while the most energetic is along the W direction, thus both Higgses end up forming a small invariant WH mass.

There are other types of diagrams that, especially for the heavy Higgs mass, are dominating. These are the fusion type diagrams where each photon splits into two W , the external outgoing W (spectator W) going very forward and taking a large amount of energy as we saw. The other, internal W , takes part in the hard process and triggers $WW \rightarrow HH$. If these internal W 's are quasi-real (almost on shell) than the t-channel diagrams are every much enhanced. To bring this important feature into prominence we introduce the variables X_{\pm} that measure the virtuality of the fusing W 's. $X_+ = (m_W^2 - q_+^2)/s$, where $q_+ = p_{\gamma_1} - p_{W^+}$, ($q_+^2 = -Q_+^2$) and $X_- = (m_W^2 - q_-^2)/s$ with $q_- = p_{\gamma_2} - p_{W^-}$. When the W^+ is emitted with high energy in the ‘‘parent’’ photon direction, the variable X_+ is very small. The dominance of the fusion diagrams is well rendered by Fig. 11 that clearly shows that the bulk of the events originate from a very small region of phase space tightly clustered around both $X_{\pm} \sim 0$. It should also be noted that for very light Higgs, when it is emitted either along the W direction or with little energy (essentially a bremsstrahlung Higgs) the variables X_{\pm} calculated for the bremsstrahlung diagrams can also be small. This observation of the importance of the fusion diagrams, referred to earlier, will become crucial when we will derive a high energy approximation for the process.

The above distributions together with the discussion we had on the Higgs mass de-

Figure 8: *Angular distribution of the least and most energetic Higgses with respect to the beam .*

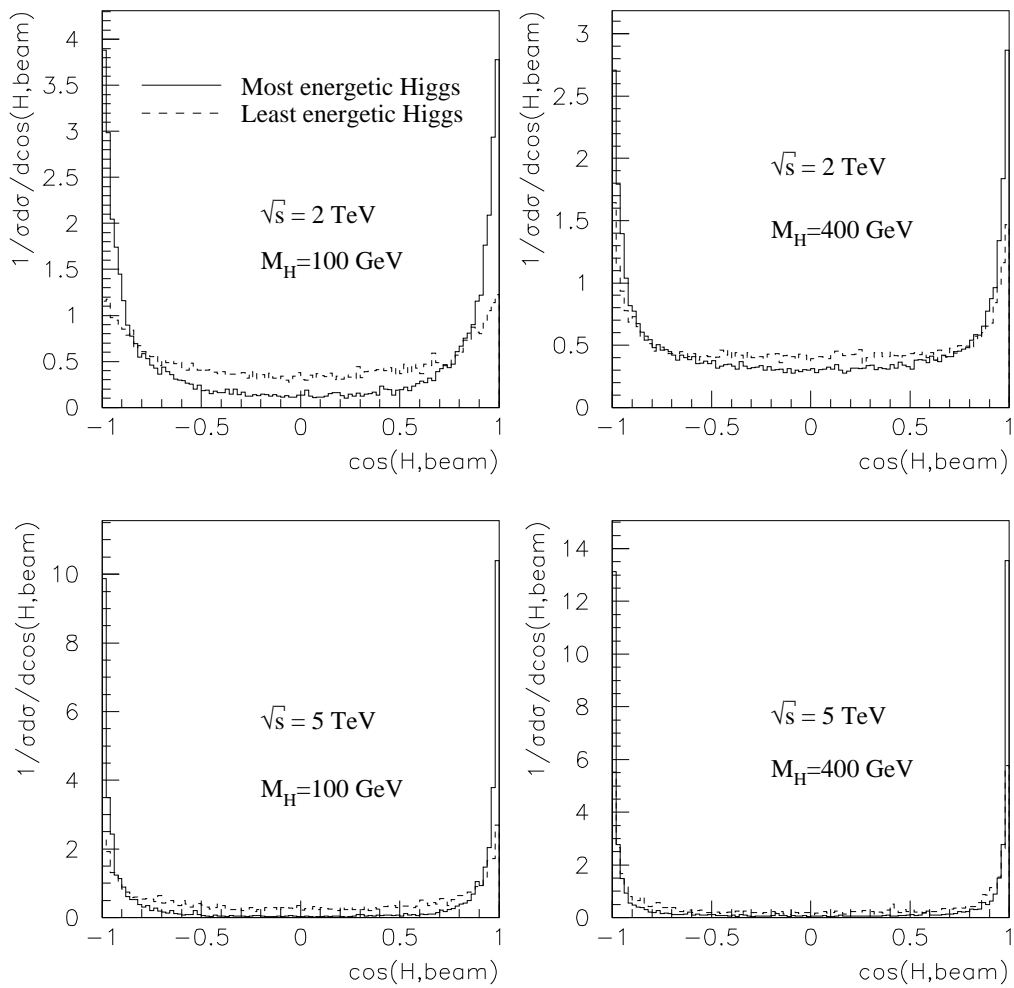


Figure 9: *Energy distribution of the W for different Higgs masses at two typical energies. Both the transverse and the longitudinal W distributions are shown.*

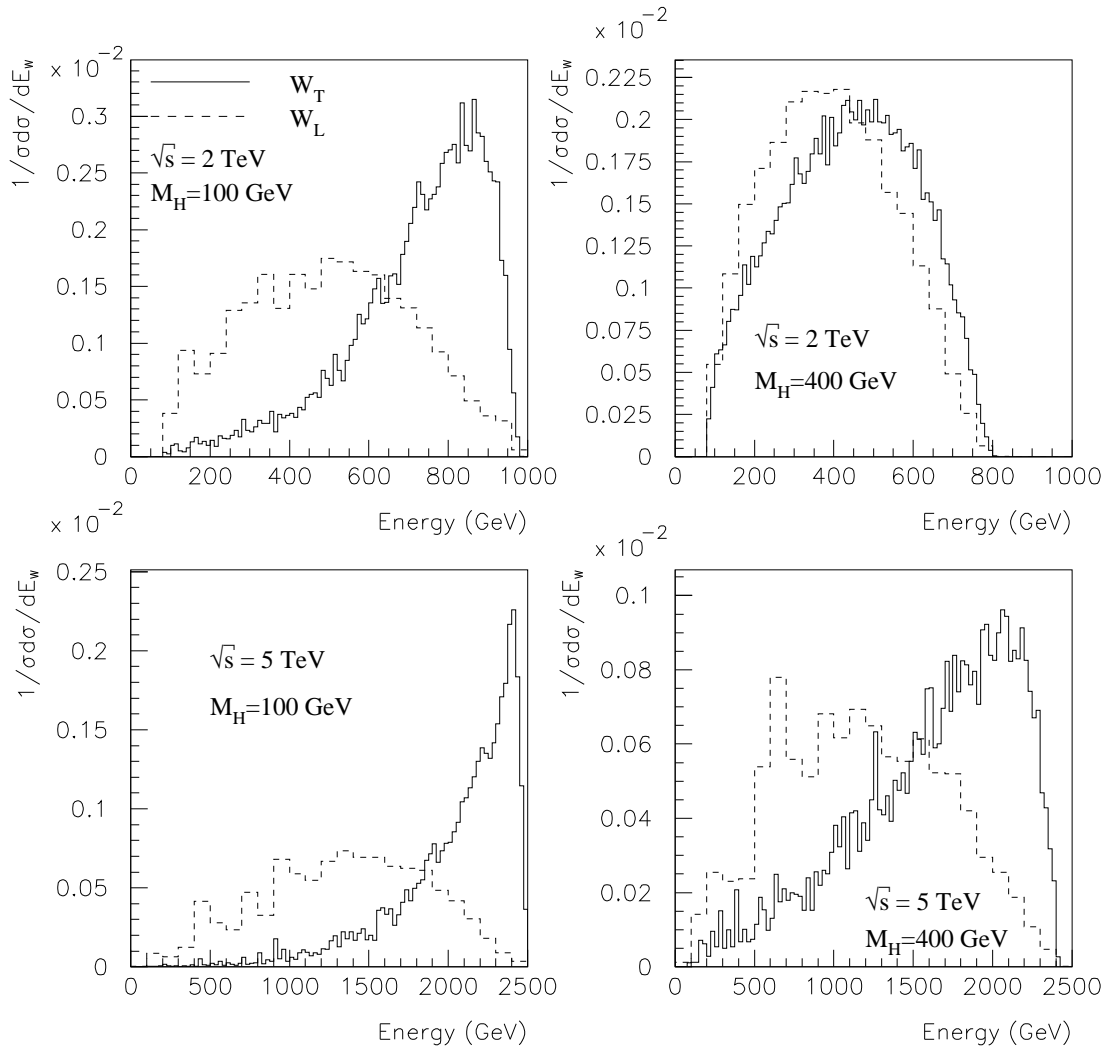
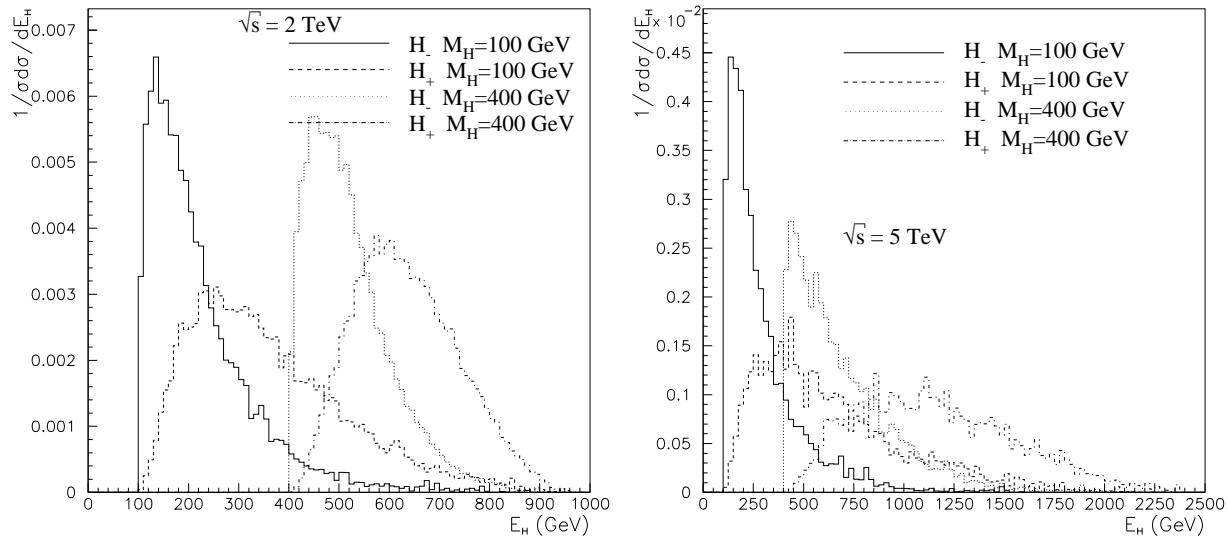


Figure 10: *Distribution in the energy of the least energetic (H_-) and the most energetic (H_+) Higgs.*



pendence are an indication that the leading topology is one with both outgoing W being transverse. They are emitted very forward along the beam hence forcing the intermediate W 's to be quasi-real especially at high energies. All these characteristic are consistent with an interpretation, especially for heavy Higgs, in terms of the dominance of fusion diagrams with the photon splitting into a spectator W_T (transverse) and another W that takes part in the hard scattering process $W^+W^- \rightarrow HH$. We will see in section 4 that this is dominated by $W_L W_L$. From a previous study[12, 11] we have given formulae for the structure function describing a W_L inside a photon (see below also), these lead to an effective $W_L W_L$ luminosity that falls like $1/\hat{s}$, where \hat{s} is the invariant mass of the $W_L W_L$ subsystem. We thus should expect that the largest contribution to the total cross section to come from values of the invariant M_{HH} mass not too far from threshold, if indeed the fusion diagrams contribute substantially. As fig. 12 confirms, the average invariant mass is not sensibly above threshold especially for a heavy Higgs. For a light Higgs the invariant mass of the Higgs system is only a fraction of the total energy.

3 Comparison with other processes at the linear colliders

Figure 11: *Double distribution in the reduced variables X_{\pm} that measure the virtuality of the fusing W 's.*

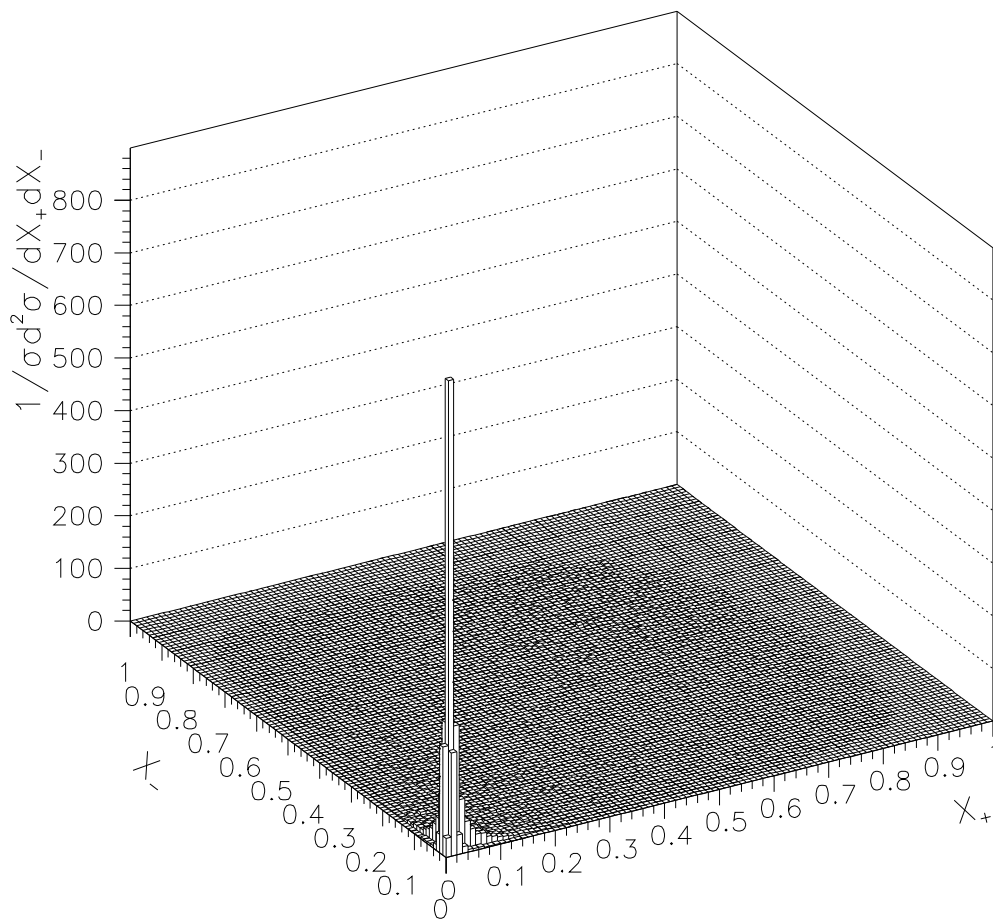
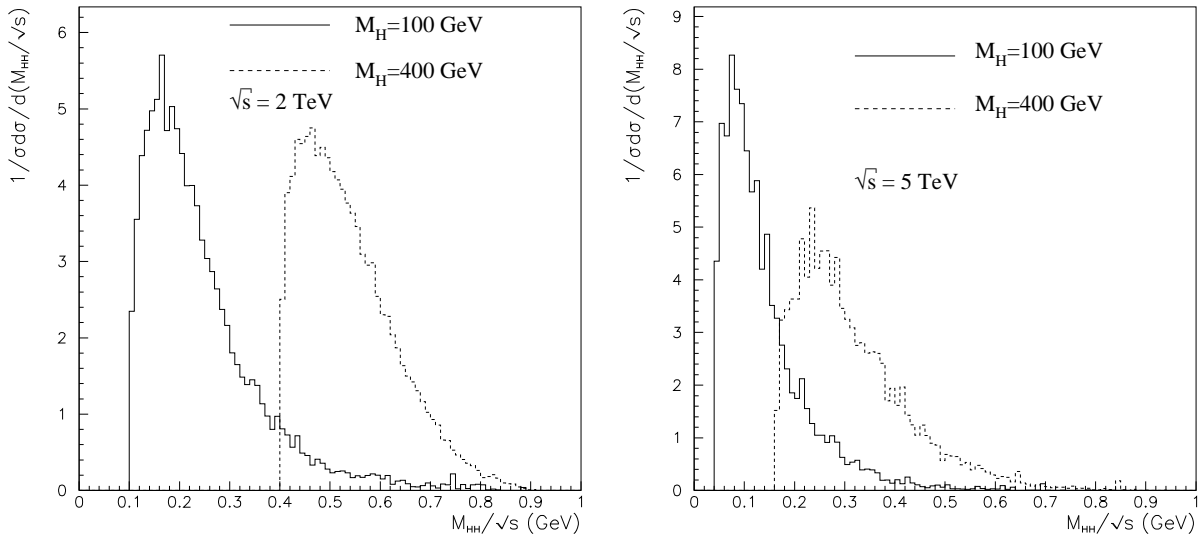


Figure 12: *Distribution in the reduced invariant mass of the Higgs system for $M_H = 100, 400\text{GeV}$ and $\sqrt{s} = 2\text{TeV}, 5\text{TeV}$.*

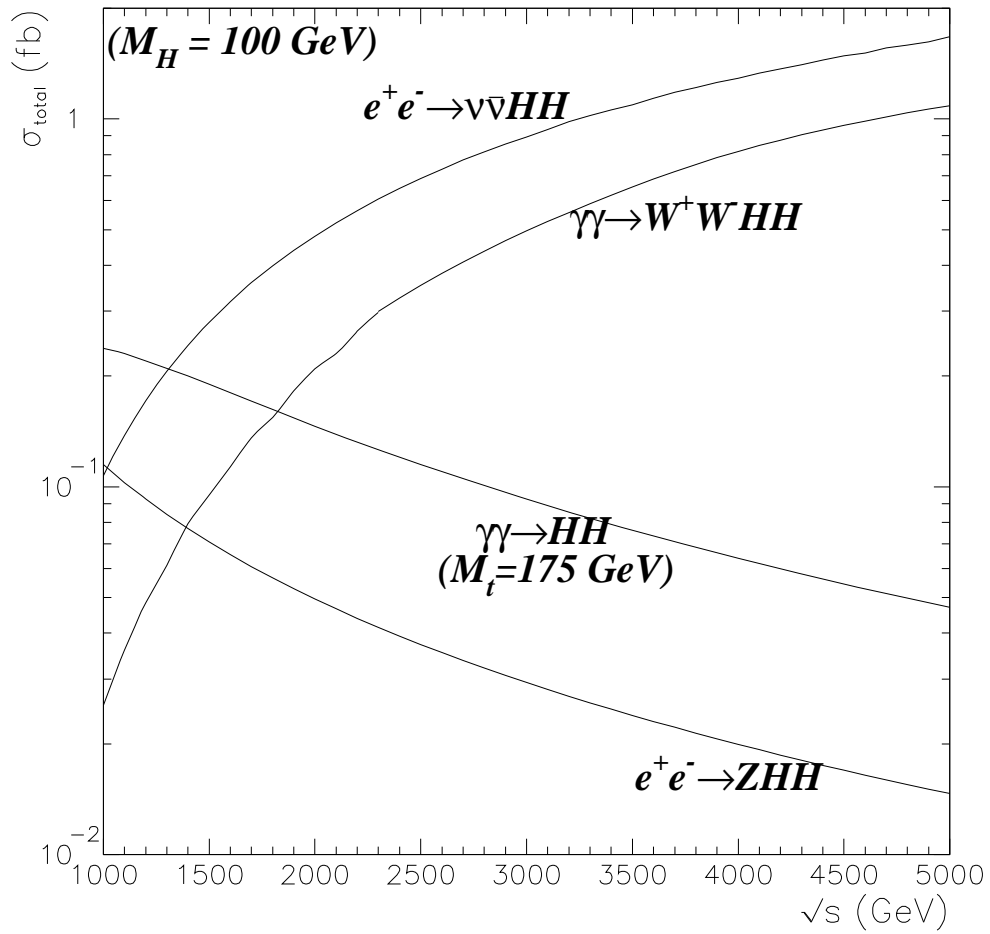


3.1 Light Higgs at e^+e^- colliders

At the same order in the coupling constants as the process we are studying, double Higgs production can be generated at the loop level via $\gamma\gamma \rightarrow HH$ and could allow the probing of the triple Higgs vertex[5]. However, this test will have to rely on a very precise value of the $H \rightarrow \gamma\gamma$ branching ratio. At a 2TeV cms energy the cross section is of the same order as the $WWHH$ production for a Higgs mass of 100GeV. When one is not penalised by phase space $WWHH$ production is larger, for instance at 5TeV there is an order of magnitude between the two cross sections. The equivalent loop-induced double Higgs production in e^+e^- has been found to be much too small[15], at best it has a cross section of 0.1fb and decreases quickly with energy. However the most efficient means for double Higgs production in the e^+e^- mode is via WW fusion leading to $e^+e^- \rightarrow \nu_e\bar{\nu}_e HH$. The double Higgs bremsstrahlung ($e^+e^- \rightarrow ZHH$) is only competing at relatively low energies where the event sample is too low to be useful. We have recalculated the $e^+e^- \rightarrow \nu_e\bar{\nu}_e HH$ cross section. As Fig. 13 shows, $e^+e^- \rightarrow \nu_e\bar{\nu}_e HH$ exhibits the same logarithmic growth and is slightly larger than $\gamma\gamma \rightarrow W^+W^- HH$ for the same cms[‡]. This is partly due to the larger phase space allowed for the e^+e^- process. Another reason

[‡]We have not counted the part $e^+e^- \rightarrow HHZ \rightarrow HH\nu_e\bar{\nu}_e$ with the fusion diagrams

Figure 13: Comparison of cross sections for double Higgs production at e^+e^- and $\gamma\gamma$ reactions for a light Higgs $M_H = 100\text{GeV}$.



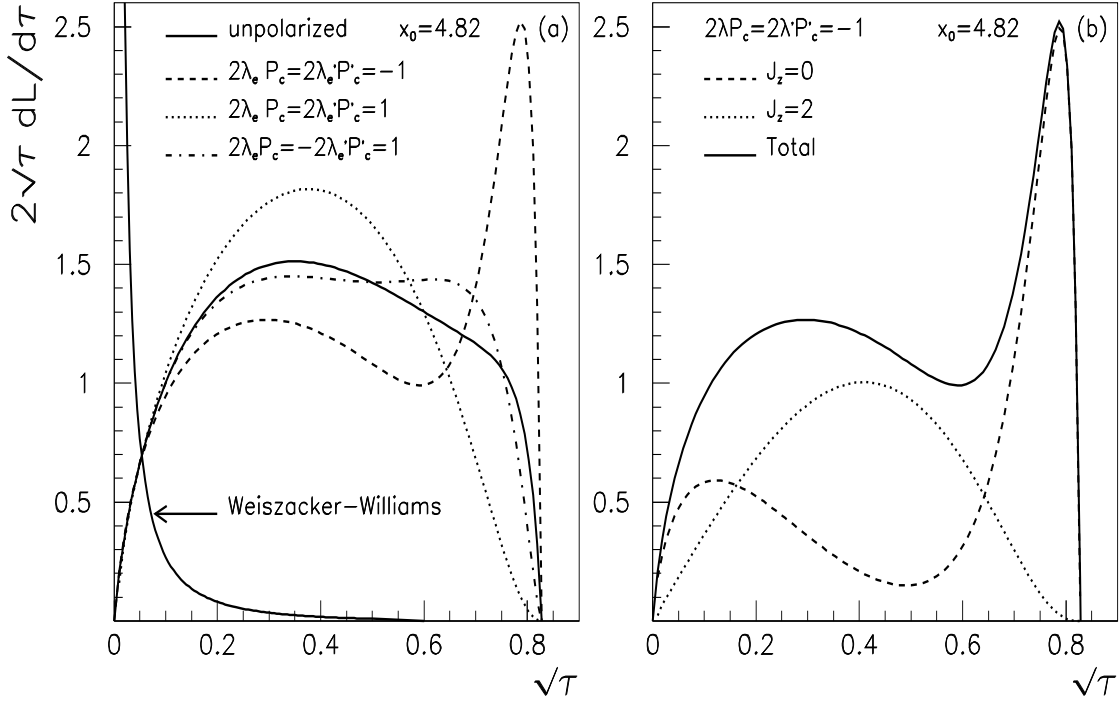
is that the $e^+e^- \rightarrow \nu_e\bar{\nu}_e HH$ cross section could be interpreted solely in terms of the fusion of WW that rescatter into HH , while the equivalent $\gamma\gamma$ involves bremsstrahlung type diagrams that for a light Higgs $\sim M_W$ interfere destructively with the fusion type diagrams. Note that these fusion type diagrams $WW \rightarrow HH$ are also common to the loop induced $\gamma\gamma \rightarrow HH$ and $e^+e^- \rightarrow HH$. This last remark also explains why $\gamma\gamma \rightarrow HH$ is larger than $e^+e^- \rightarrow HH$, $\gamma\gamma \rightarrow W^+W^-$ is about an order of magnitude larger than $e^+e^- \rightarrow W^+W^-$ [§]. This said, all mechanisms for double Higgs production give, for the foreseeable future colliders, a cross section that is below .5fb for the light Higgs scenario with the largest cross section occurring in the classic e^+e^- . The yield of double Higgs can be even larger in the e^+e^- mode. If both the e^+ and e^- are polarised one can gain as much as a factor of four! No such beefing up can occur in the $\gamma\gamma$ mode as all combinations of the photon polarisations give sensibly the same values as shown earlier. If anything, $\gamma\gamma$ cross sections will suffer some reduction when one takes the photon spectra into consideration.

3.2 Convoluting with the photon luminosity spectra

At this point it is necessary to discuss how the cross section for double Higgs production in $\gamma\gamma$ is affected by including the photon luminosity spectra. The colliding high energy photons are obtained by Compton backscattering of an intense laser light on the single-pass electrons. The spectra used by almost all physics analyses till now have been based on the much advertised luminosity functions of[2]. Nearly all studies have considered that the conversion point coincided with the interaction point. By increasing the conversion distance one obtains more monochromatic spectra peaked towards the highest possible energy but one loses in luminosity as the softer converted photons would not reach the interaction point. To make the comparison with other physics studies conducted for these types of machines we will only illustrate the case with a zero conversion distance and with a parameter for the setting that allows the highest possible centre-of-mass energy and yet does not trigger electron pair production through the interaction of a laser photon and a converted photon. This corresponds to the parameter $x_0 = 4.8$ [2, 12] and means that centre-of-mass energies up to 83% of the original e^+e^- can be reached. The issue of polarisation is crucial. Figure 14 shows that by choosing the circular polarisation of the laser, P_c , and that of the corresponding electron, λ_e , such that for both ‘‘arms’’ of the colliders one has $2\lambda_e P_c = 2\lambda'_e P'_c = -1$ one obtains a peaked spectrum toward the highest τ : $\tau = s_{ee}/s_{\gamma\gamma}$. For this peaked spectrum one also sees that if one takes $P_c = P'_c = +1$ then the produced hardest photons are mainly in the $J_Z = 0$. For our process where we

[§]Another reason, is that $\gamma\gamma \rightarrow HH$ receives an important contribution from the top.

Figure 14: (a) Photon-photon luminosity spectra for different polarisation of the laser beams P_c (circular) and the electrons λ_e of the linac. (b) shows the relative contribution of the $J_Z = 0$ and the $J_Z = 2$ luminosities.



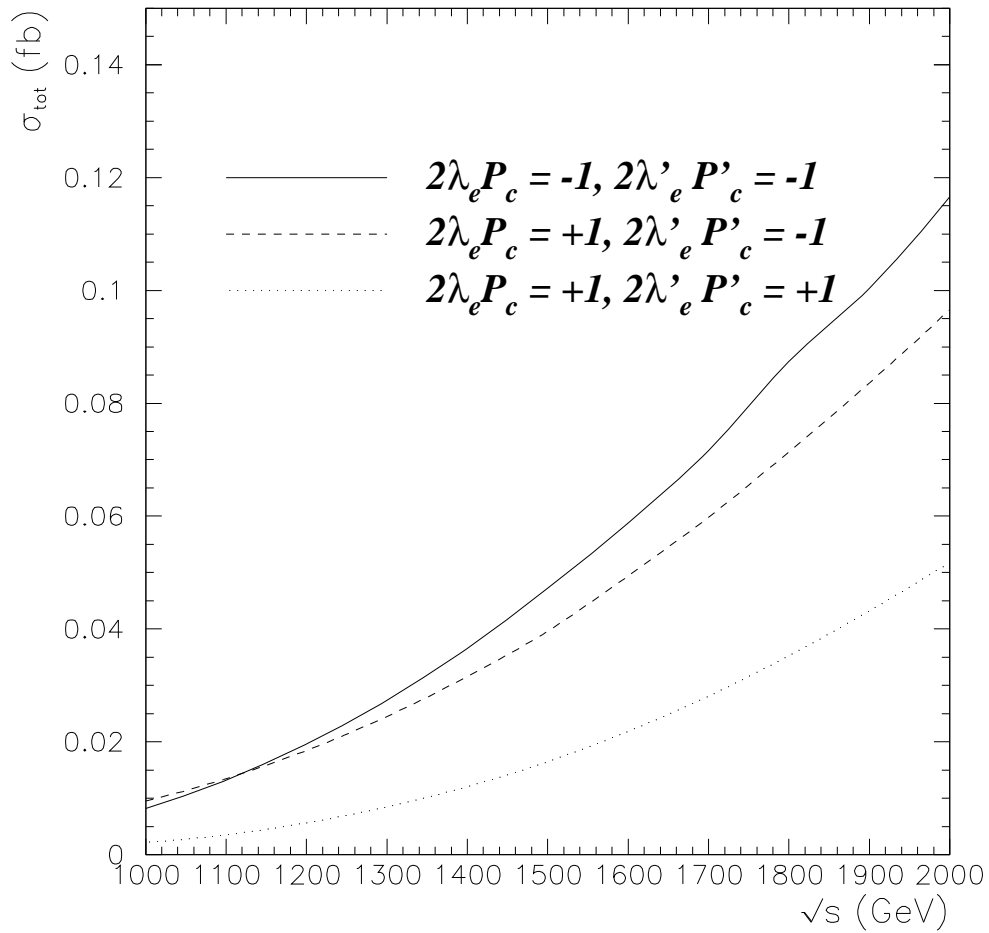
need to be at the highest possible $s_{\gamma\gamma}$ it is clear that we should prefer a peaked spectrum. Selecting between a $J_Z = 0$ and a $J_Z = 2$ dominated spectrum is not terribly important as the process depends very little on the initial polarisation.

It has very recently been realised[23] that taking into account multiple scattering and non-linear effects these “ideal” spectra are disrupted. The main characteristic is that the luminosity at the higher end of the spectra is lowered while one has an increase in the luminosity of the soft photons. The detailed Monte Carlo simulations [23] depend quite critically on the parameters of the beams etc., but because of the typical spectra arrived at, it would be a good approximation to assume that one has an almost monochromatic spectrum peaked at the highest possible $\sqrt{s_{\gamma\gamma}}$ energy but with a luminosity of about a factor 2-5 lower than the original e^+e^- [23].

For our process, convoluting with the “ideal” spectrum ¶ we find in fact that at 2TeV e^+e^- cms energy and for a Higgs mass of 100GeV the cross section with the peaked spec-

¶ This is technically more time consuming as it introduces yet two more integration variables.

Figure 15: The $\gamma\gamma \rightarrow W^+W^-HH$ cross section after convoluting with the “ideal” luminosity spectra for different combinations of the polarisations of the electrons and the laser. The Higgs mass has been set at 100GeV.



trum drops by about at least a factor of 2 compared with the result without convolution, see Fig. 15. Of course it is worse by a factor 4 if the broad spectrum $2\lambda_e P_c = 2\lambda'_e P'_c = 1$ is taken. Therefore, we see that had we taken the preliminary results on the spectra that take into account multiple scattering etc, that suggests to include a factor 2 (at least) reduction in the $\gamma\gamma$ luminosity we would have obtained the correct order of magnitude of the convoluted cross section.

Comparing now the $\gamma\gamma \rightarrow W^+W^-HH$ with double Higgs production in e^+e^- for the foreseeable colliders it is clear that the yield of double Higgs is larger at the e^+e^- option by at least a factor 2. In real life, there could easily be an order of magnitude between the two yields considering the availability of polarisation.

3.3 Higgs mass dependence of the $e^+e^- \rightarrow \nu_e\bar{\nu}_e HH$ cross section

One revealing characteristics that we observed in the $\gamma\gamma \rightarrow W^+W^-HH$ was that the accuracy in the probing of the triple Higgs vertex was acutely dependent on the mass of the Higgs since there was destructive interference between the signal diagrams that contain the triple vertex and the rest. This destructive interference becoming more severe as the mass increases. As figures 16 show, this feature is still present and it therefore confirms that the background diagrams though not containing the HHH vertex do get balanced out by the $W_L W_L HH$. This is a suggestion that the quasi-real W's are preferentially longitudinal. As we will see, $WW \rightarrow HH$ is essentially triggered by the longitudinal W. Therefore we have strong indications to suspect that the whole cross section can be well recovered by the effective W_L approximation. Another supporting evidence is that this approximation has been shown to work very (rather) well for a heavy (light) Higgs for pp reactions at $40TeV$ [24]. Moreover, as Fig. 17 indicates the invariant mass of the HH system is, for high enough energy, clustered around small values of this invariant mass so that the effective W_L approximation (EWA) should work quite well.

3.4 Heavy Higgs

The comparison between all mechanisms for double Higgs production when the Higgs is heavy very much favours $\gamma\gamma \rightarrow W^+W^-HH$ as soon as phase space factors (due to the accompanying W pair) are negligible. For the 2TeV collider and a 400GeV Higgs, there is enough phase space to make $\gamma\gamma \rightarrow W^+W^-HH$ larger than $e^+e^- \rightarrow \nu_e\bar{\nu}_e HH$, though both cross sections are far too small, but not enough for $\gamma\gamma \rightarrow W^+W^-HH$ to

Figure 16: Dependence of the $e^+e^- \rightarrow \nu_e \bar{\nu}_e HH$ cross section on the Higgs mass at 2TeV and 5TeV. The relative contributions of the signal diagrams containing the H triple vertex and the background are shown.

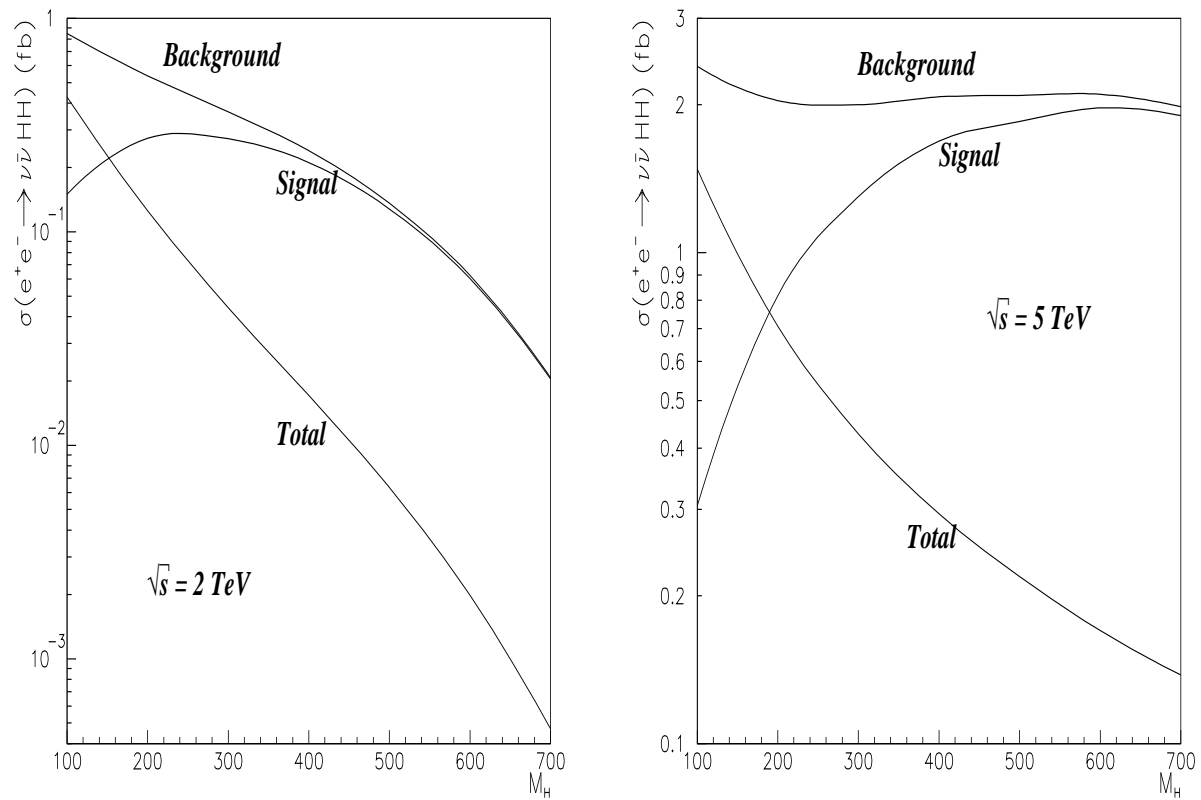


Figure 17: *Distribution in the reduced invariant mass of the HH system for $M_H = 100, 400\text{GeV}$ and $\sqrt{s} = 2\text{TeV}, 5\text{TeV}$.*

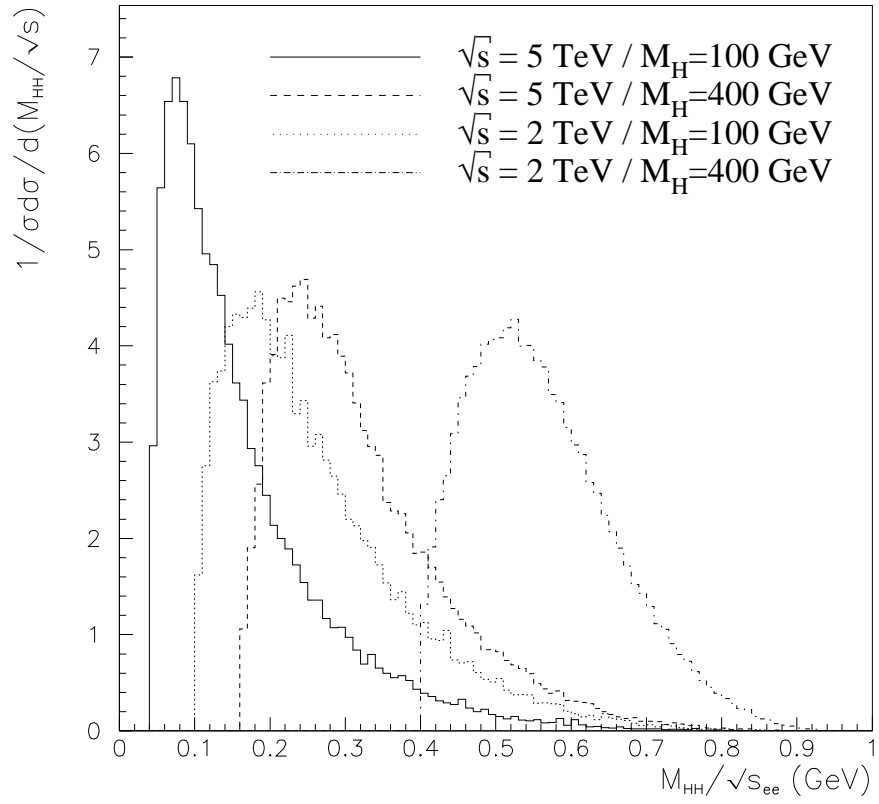
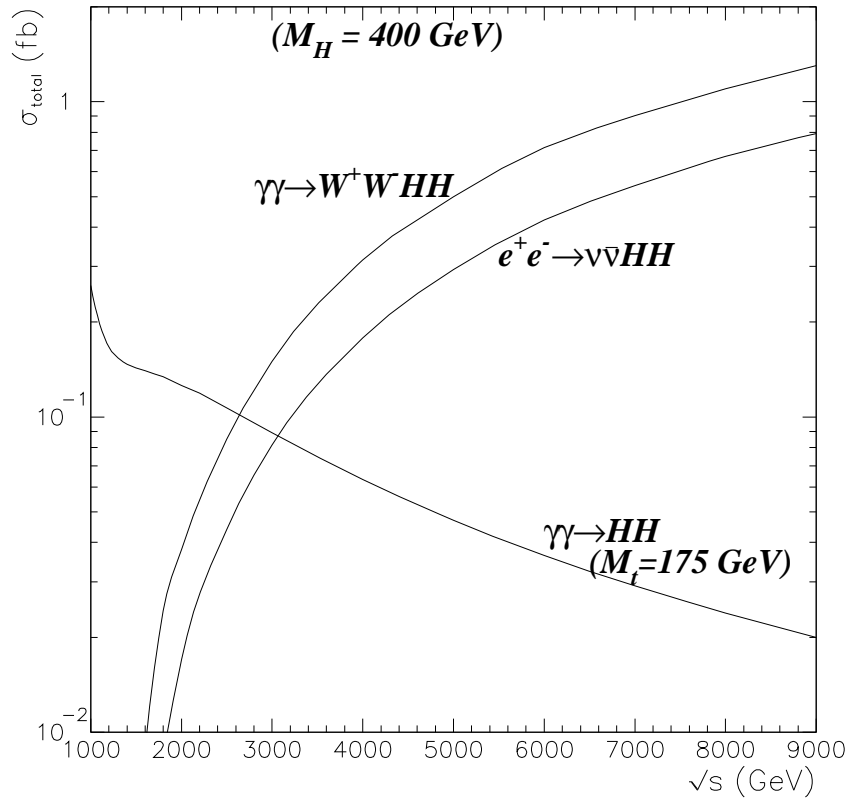


Figure 18: *Energy dependence of the main cross sections for double Higgs production for a heavy Higgs.*



be the dominant cross section. The loop-induced $\gamma\gamma \rightarrow HH$ [5] is larger and could be measurable. However, very quickly $\gamma\gamma \rightarrow W^+W^-HH$ takes over and one sees that it becomes the main mode for double Higgs production already at $3TeV$ (see Fig. 18).

4 The structure function approach and $W^+W^- \rightarrow HH$

In order to check whether the equivalent W approximation works, one needs to know not only the distributions of the W inside the electron and the photon but also the behaviour of the hard process, which for the case at hand is $W^+W^- \rightarrow HH$. We will see that it is dominated, by far, by the longitudinal W 's in which case it is sufficient to only use the longitudinal W distribution function.

4.1 $W^+W^- \rightarrow HH$

The amplitude for the process $W_L W_L \rightarrow HH$ has been calculated before [24]. We have recalculated this amplitude by also allowing for the triple Higgs vertex to have a value different from that in the \mathcal{SM} and have derived the other helicity amplitudes. We take the H^3 vertex to have a strength h_3 times of what it is in the \mathcal{SM} (see next section). Denoting the velocities of the W and H as $\beta_{W,H} = \sqrt{1 - 4M_{W,H}^2/s}$, we introduce the ‘‘enhanced coupling’’ $r = M_H^2/M_W^2$ while we define $x_0 = (1 + \beta_H^2)/2\beta_W\beta_H$. x is the cosine of the scattering angle θ : $x = \cos\theta$. We find

$$\begin{aligned} \tilde{\mathcal{M}}_{LL} &= \frac{g^2}{2} \left\{ \frac{1}{\beta_H\beta_W^3} \left(\frac{1}{x-x_0} - \frac{1}{x+x_0} \right) \left(r\frac{M_H^2}{s} + \beta_H^2 + \beta_W^4 \right) \right. \\ &\quad \left. + \frac{1}{\beta_W^2} (2 - \beta_W^2 - r) + \frac{3h_3r}{4} \left(\frac{1 + \beta_W^2}{1 - M_H^2/s} \right) \right\} \end{aligned} \quad (4.1)$$

It is important to note that there is a cancellation between the terms of enhanced strength $\propto r = M_H^2/M_W^2$, as pointed out in section 2:

$$\tilde{\mathcal{M}}_{LL} \rightarrow \frac{g^2}{4} r (3h_3 - 2) + \dots \quad (4.2)$$

The term in h_3 comes solely from the s-channel and for the \mathcal{SM} values there is indeed a cancellation, though not complete. We clearly see here that if there is a deviation in the \mathcal{SM} value, it is made more conspicuous for higher values of the Higgs mass, since the terms in the anomalous couplings are enhanced as the Higgs mass increases.

Obviously the h_3 dependence only occurs for like-sign W helicities. Thus the remaining transverse modes that do not have an enhanced coupling factor r are not so conducive to testing these couplings. The other helicity amplitudes are

$$\begin{aligned} \tilde{\mathcal{M}}_{+L} &= \frac{g^2}{4\beta_W^2} \sqrt{\frac{2M_W^2}{s}} \sin\theta \left(\frac{1}{x-x_0} + \frac{1}{x+x_0} \right) (r-2) \\ \tilde{\mathcal{M}}_{+-} &= g^2 \frac{\beta_H}{4\beta_W} \sin^2\theta \left(\frac{1}{x-x_0} - \frac{1}{x+x_0} \right) \\ \tilde{\mathcal{M}}_{++} &= g^2 \left\{ \frac{1}{\beta_H\beta_W^3} \left((2\beta_W^2 - \beta_H^2) \frac{M_W^2}{s} - \left(\frac{M_H^2}{s} \right)^2 \right) \left(\frac{1}{x-x_0} - \frac{1}{x+x_0} \right) \right. \\ &\quad \left. + \frac{2\beta_W^2 - \beta_H^2 - 1}{4\beta_W^2} + \frac{3h_3}{2} \frac{M_H^2}{s} \left(\frac{1}{1 - M_H^2/s} \right) \right\} \end{aligned} \quad (4.3)$$

As Figures 19 show the cross sections are indeed essentially produced through both W being longitudinal, for both a light and a heavy Higgs. Nonetheless the leading contribution at high energies is from the t-channel W diagrams and comes from the W being extremely forward. The asymptotic form of the total cross section is not sensitive to the H^3 coupling and is given by

$$\begin{aligned}
\sigma_{LL} & \xrightarrow{s \gg M_H^2, M_W^2} \sigma_\infty \equiv \frac{\pi\alpha^2}{s_W^4} \frac{1}{4m_W^2} \\
\sigma_{TL} & \xrightarrow{s \gg M_H^2, M_W^2} \frac{M_W^2}{2s} \frac{M_H^2 - 2M_W^2}{s} \left(\ln(s/M_W^2) - 3 \right) \sigma_\infty \\
\sigma_{TT} & \xrightarrow{s \gg M_H^2, M_W^2} \frac{M_W^2}{4s} \sigma_\infty
\end{aligned} \tag{4.4}$$

To bring the effect of the H^3 coupling into prominence a cut on the forward/backward directions is essential. Introducing an angular cut θ_0 , such that all Higgses within this angle (measured with respect to the W direction) are rejected, and with $2M_W/\sqrt{s} \ll \theta_0 \ll 1$, the leading behaviour becomes very sensitive to the value of the triple Higgs vertex. To wit, with $r \gg 1$

$$\sigma_{LL} \sim \frac{\pi\alpha^2}{s_W^4} \frac{1}{16s} \left(\frac{M_H^2}{M_W^2} \right)^2 (3h_3 - 2)^2 \tag{4.5}$$

Note also that the $W_L W_L$ cross section is dominant even after angular cuts are applied, see Fig. 19.

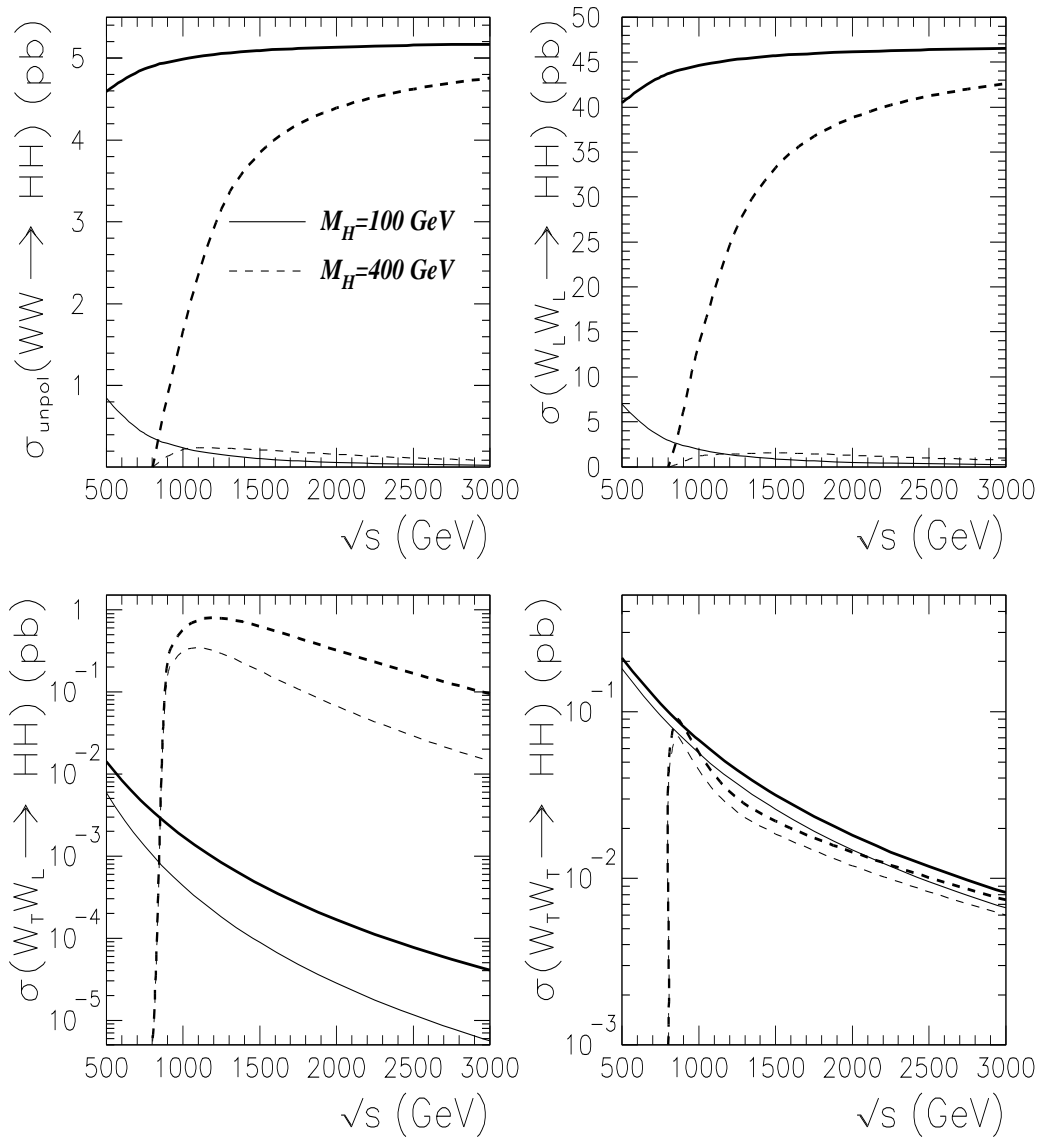
Having confirmed the overwhelming dominance of the $W_L W_L$ cross section, we now turn to a discussion on the structure functions of the W_L inside the electron and photon.

4.2 Comparisons between the distribution functions for the W_L inside the electron and the photon

There have been numerous derivations of the distribution (or structure function) of the W inside the light fermions (quarks and electrons) [10]. For the effective W approximation, the most interesting aspect concerns the W_L content, which in combination with the equivalence theorem[22] has been used to investigate manifestations of models of symmetry breaking and Higgs production. All the available distributions reproduce the same leading function that exhibits scaling behaviour. For the *unpolarised* electron one has

$$D_{W_L/e}(y) = \frac{\alpha}{4\pi s_W^2} \frac{1-y}{y} \tag{4.6}$$

Figure 19: Energy dependence of the $W^+W^- \rightarrow HH$ cross section. The different helicity contributions are shown for comparison against the unpolarised cross section. Thick lines are for the total cross sections while the thin lines correspond to a cut on the scattering angle with $|\cos\theta| < 0.8$.



where y is the momentum fraction of the electron transferred to the W .

The W_L distribution inside the photon has only very recently been studied [11, 12, 19]. This distribution consists of two different parts. The first represents the situation where the spectator W^\parallel is transverse. The second component takes into account the contribution of the longitudinal spectator W . The latter does not have an equivalent in the fermion splitting case. As for the former we have shown that [12], modulo an overall factor, it has the same universal structure as the one for the electron

$$D_{W_L/\gamma\lambda}^{(W_\lambda)}(y) = \frac{\alpha}{\pi} \frac{1-y}{y} \quad (4.7)$$

Note that in this case the photon transfers its helicity, λ , to the spectator W . The contribution from the W with the opposite helicity, $-\lambda$, is non leading. One important difference with the electron case is that whatever the helicity of the photon one gets the same probability for having a W_L . Thus we may just as well write the *unpolarised* distribution:

$$D_{W_L/\gamma}^{(W_T)}(y) = \frac{\alpha}{\pi} \frac{1-y}{y} \quad (4.8)$$

As for the spectator- W_L component we have shown [12] that an approximation that works very well for $\gamma\gamma \rightarrow W^+W^-H$ is

$$D_{W_L/\gamma\lambda}^{(W_L)}(y, Q_p^2) = \frac{\alpha y(1-y)}{\pi} \frac{1}{2} \left(-2 + \ln \frac{Q_p^2}{M_W^2} \right) \quad (4.9)$$

Where Q_p^2 is a typical Q^2 value for the hard process. Despite its Q_p^2 *logarithmic* enhancement this contribution is only a fraction of the W_T component as evidenced by the fact that the yield of external W_L 's is always an order of magnitude below that of the transverse. We will not consider the contribution from this component in the present paper, therefore when looking at the validity of the approximation we will only compare it with the doubly transverse exact $\gamma\gamma \rightarrow W^+W^-HH$ cross section that may also be compared to the equivalent $e^+e^- \rightarrow \nu_e\bar{\nu}_eHH$.

The issue of the W_L content of the photon is of importance. Since one of the aims of the $\gamma\gamma$ colliders is to study symmetry breaking, it is essential to know whether $\gamma\gamma$ collisions can yield a higher luminosity in W_LW_L . Looking at the W_L distributions in both the photon and the electron one is tempted to conclude that there are equally as many W_L in the photon as in the electron. However, the photon being “democratic” produces,

^{||}The one that does not take part in the hard scattering and plays the role of the neutrino in the electron case.

regardless of its polarisation, both W^+ and W^- with an equal probability. We can then study $W_L^\pm W_L^\pm$, while only $W_L^+ W_L^-$ is possible in e^+e^- . Moreover, for the latter channel (W^+W^-) one gains a factor of two in the $\gamma\gamma$ mode. However, we should not forget that one has to take into account the convolution with the real spectra, moreover for the structure function approximation to be trusted one needs to go to a regime where the W mass can be neglected, since in $\gamma\gamma$ one has less phase space. Furthermore, we have seen that, in order to have a $\gamma\gamma$ luminosity peaked at high values of the $\gamma\gamma$ centre-of-mass, polarisation of the electron was essential. Now, if one polarises the electrons in the e^+e^- mode to be left-handed (and the positrons right-handed), one gains a factor of 4 in the e^+e^- convolution. Therefore, it is fair to argue that there could be a complementarity as different channels for effective WW scattering are open ($W^\pm W^\pm, W^+W^-$) in the $\gamma\gamma$ mode, but it is far from certain that the effective luminosity after convolution with the $\gamma\gamma$ spectra will be enough for the foreseeable future colliders to fare better in the $\gamma\gamma$ than the e^+e^- mode.

4.3 Approximating the $e^+e^- \rightarrow \nu_e \bar{\nu}_e HH$ cross section

We are now in a position to evaluate the $e^+e^- \rightarrow \nu_e \bar{\nu}_e HH$ cross section through the effective W_L inside the electron:

$$\begin{aligned} \sigma_{e^+e^- \rightarrow \nu_e \bar{\nu}_e HH} &\simeq \int_{4M_H^2/s}^1 d\tau \int_{\tau/y_m}^{y_m} \frac{dy}{y} D(y) D(\tau/y) d\sigma(W_L W_L \rightarrow HH) \\ &\simeq \int_{4M_H^2/s}^1 d\tau \mathcal{L}_{W_L^+ W_L^-}^{e^+e^-}(\tau) \sigma_{W_L W_L \rightarrow HH}(\tau s) \end{aligned} \quad (4.10)$$

with y_m the largest y allowed kinematically and where the luminosity for $W_L^+ W_L^-$ is

$$\mathcal{L}_{W_L^+ W_L^-}^{e^+e^-}(\tau) \simeq \left(\frac{\alpha}{4\pi s_W^2} \right)^2 \frac{1}{\tau} \left((1+\tau) \ln \frac{1}{\tau} - 2(1-\tau) \right) \quad (4.11)$$

where we have neglected the W mass compared to the electron energy to define the luminosity of the $W_L^+ W_L^-$ in e^+e^- .

As known and as we argued above, this effective luminosity is peaked for lower values of τ . One may try to find an analytical approximation for the $e^+e^- \rightarrow \nu_e \bar{\nu}_e HH$ total cross section since we just have one convolution to perform. We have not attempted to do this exactly. However, we have looked at how good an approximation one could obtain if one takes the constant asymptotic value for the $W^+W^- \rightarrow HH$ cross section as given by 4.4. We obtain

$$\sigma_{\infty}^{EWA}(e^+e^- \rightarrow \nu_e\bar{\nu}_e HH) \simeq \left(\frac{\alpha}{4\pi s_w^2}\right)^2 \left(\frac{1}{2} \ln^2\left(\frac{4M_H^2}{s}\right) + 2 \ln \frac{4M_H^2}{s} + 3\right) \sigma_{\infty} \quad (4.12)$$

We should not expect this additional approximation to work well as it is clear from the energy dependence of the $W^+W^- \rightarrow HH$ cross section (Figs 19), that this limiting value is quite higher than the values not far from threshold where the effective luminosity will pick up much of the cross section. Nonetheless, we should expect the energy behaviour to be fairly well reproduced as well as the order of magnitude.

We see from Figs.20 that for a Higgs mass of 100GeV, the effective W_L approximation is never within 50%, the latter attained only around 10TeV. However the energy dependence is well reproduced. For the case of the heavy Higgs the approximation is excellent, already at 2TeV it is within 10% while at 10TeV the agreement is almost perfect, reaching 3%. Very similar conclusions were obtained for the case of pp collisions at 40TeV[24]. Note that the approximation of taking the limiting high energy constant cross section (for $M_H = 400\text{GeV}$) gives a 100% overestimate.

4.4 Approximation in $\gamma\gamma \rightarrow W^+W^-HH$

Taking the distribution function for the W_L inside the photon given in 4.8 and taking into account the factor of two in the convolution we would predict $\gamma\gamma \rightarrow W_T^-W_T^+HH$ to be about $2(4s_W^2)^2$ times the $e^+e^- \rightarrow \nu_e\bar{\nu}_eHH$ cross section at high enough energy where the difference in phase space does not play a role. We have compared these two cross sections allowing for this factor. This comparison is therefore a measure of the bremsstrahlung contributions in $\gamma\gamma \rightarrow W^+W^-HH$ especially that the structure function approach in e^+e^- has been verified to be a very good approximation. The bremsstrahlung diagrams in $\gamma\gamma$ can not be deleted at a stroke since they do not form a gauge invariant sub-set, thus the comparison we propose should be a more trustworthy way of extracting the effect of bremsstrahlung. It is gratifying to see that the arguments we gave in section 2 when analysing a combination of distributions are born out by Figs. 21. We see that the effect of the genuine part of the bremsstrahlung is not negligible at all for $M_H = 100\text{GeV}$, while for $M_H = 400\text{GeV}$, their contribution gets smaller, for example it is about 30% at 8TeV. Keeping this feature in mind it is no wonder that the effective W_L does not reproduce the result as well as in the case of the e^+e^- . Nonetheless we see (Fig. 22) that for 400GeV the approximation is no worse than what it is for single Higgs production[17]. At 8TeV the cross section is reproduced within 20% of its exact value.

Figure 20: Comparing the result of the W_L effective approximation (σ^{EWA}) to the exact result σ^{exact} for $e^+e^- \rightarrow \nu_e\bar{\nu}_e HH$ for a light Higgs and a heavy Higgs. Also shown is the asymptotic analytical cross section σ_∞^{EWA} .

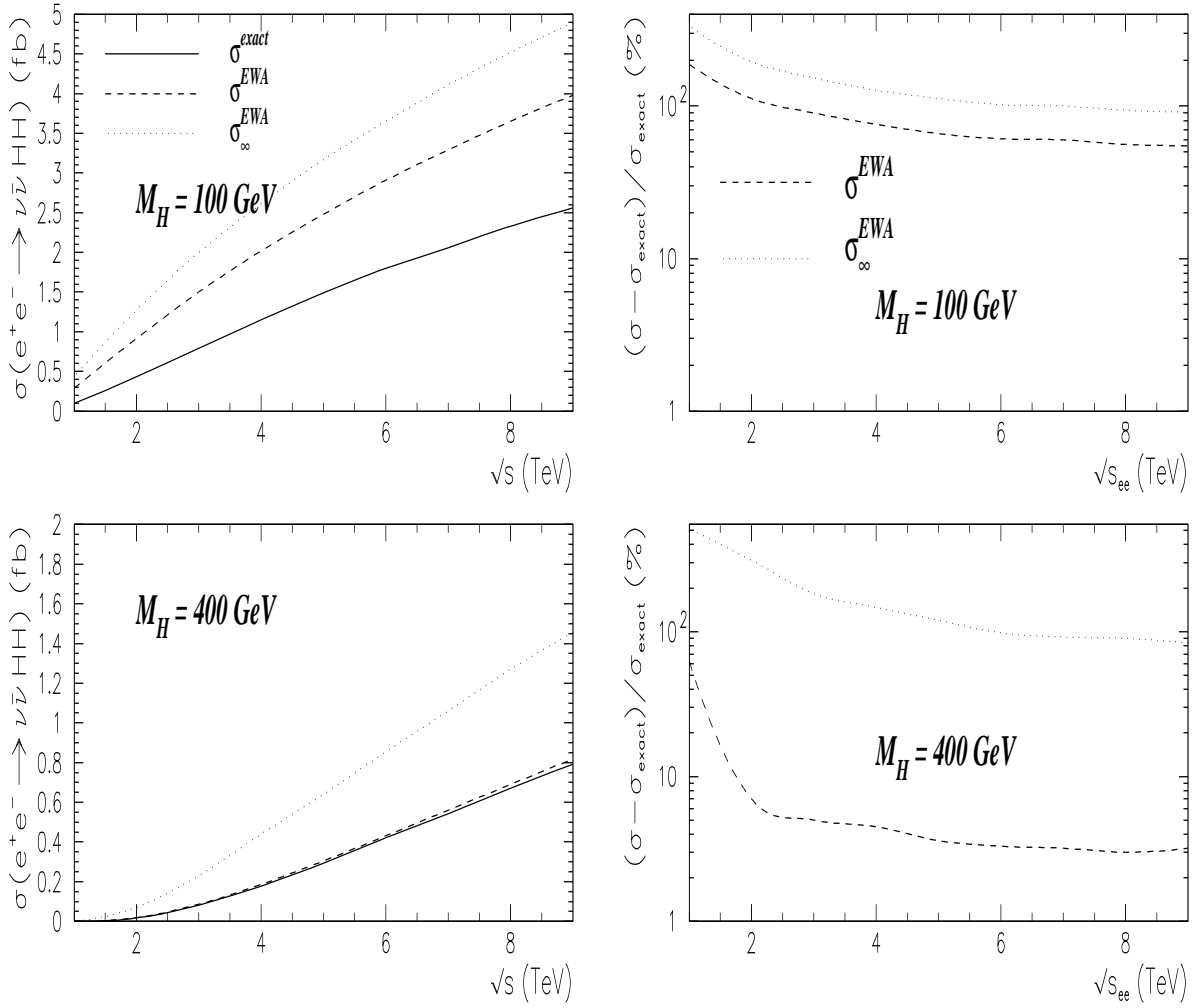


Figure 21: *The effect of the bremsstrahlung diagrams in $\gamma\gamma \rightarrow W^+W^-HH$.*

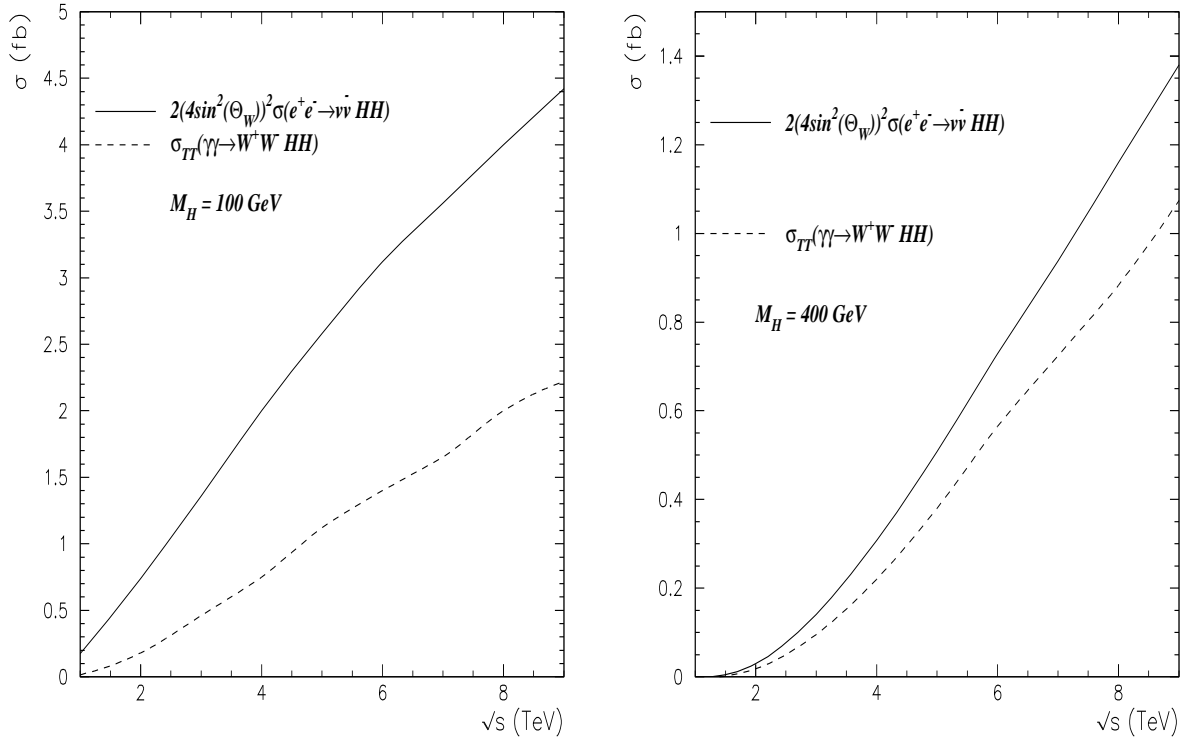
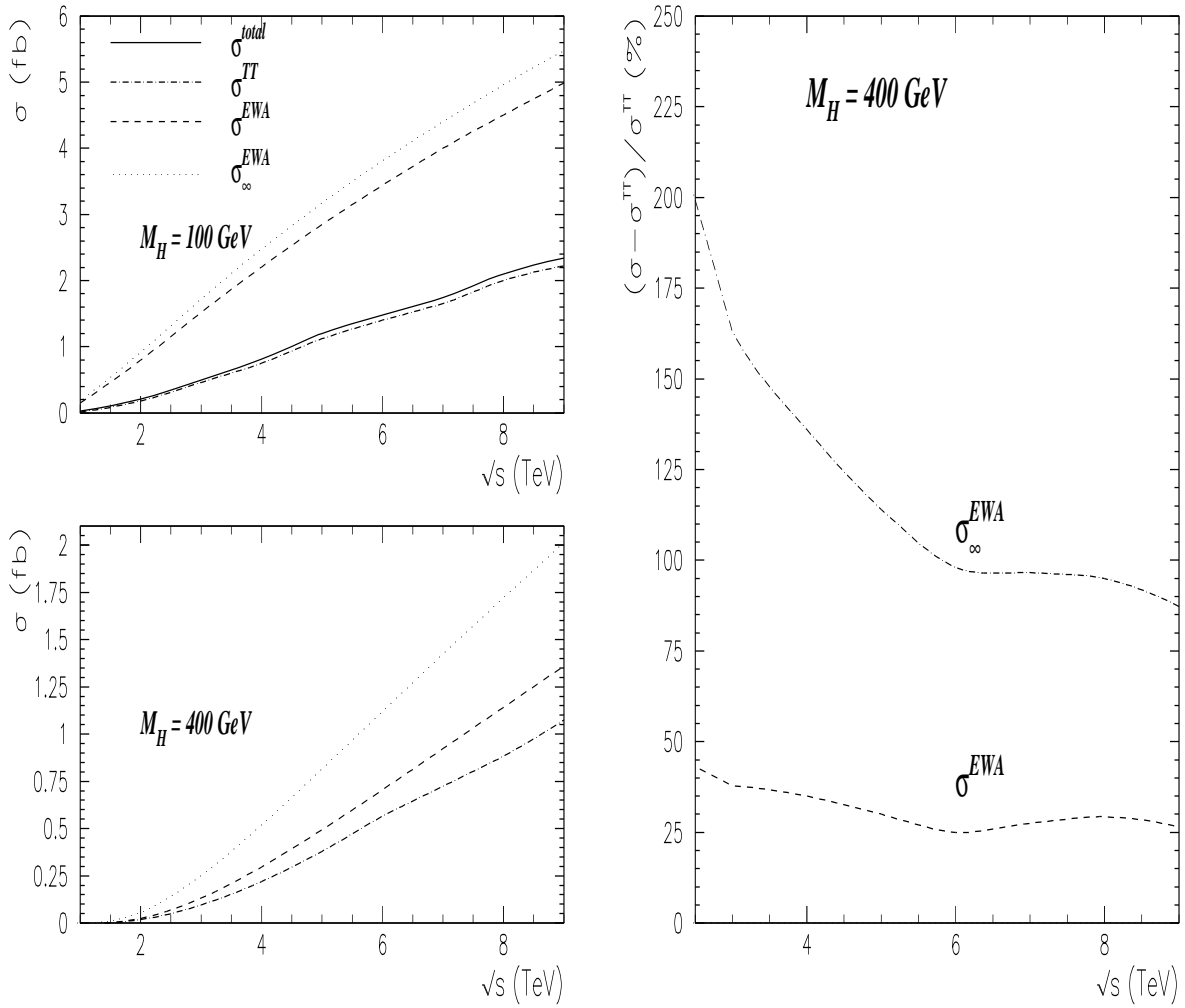


Figure 22: $\gamma\gamma \rightarrow W^+W^-HH$: comparing the result of the W_L effective approximation, σ^{EWA} , to the exact result for both W 's being transverse (σ^{TT}) for a light Higgs and a heavy Higgs. σ^{total} is the exact result including all helicity modes of the W 's. Also shown is the asymptotic analytical cross section σ_∞^{EWA} . For the heavy Higgs the percentage deviation is given.



5 Identifying and measuring the Higgs triple vertex

5.1 The triple Higgs vertex

We have, in the introduction, given ample motivation for the importance of checking the triple Higgs vertex, especially if no sign of New Physics at TeV energies has been revealed such as supersymmetry. The origin of symmetry breaking and the naturality argument would be a real puzzle, especially if only a light scalar particle has been found. One possibility, if this scalar is the Higgs, is to scrutinise the Higgs potential. Its most general form beside respecting the $SU(2)$ custodial symmetry must lead to the correct value of the vacuum expectation value[4, 5], then

$$V_{SSB} = \lambda \left\{ \sum_{n=2} \frac{g^{2(n-2)}}{\Lambda^{2(n-2)}} \frac{a_n}{(n-1)^2} \left[\Phi^\dagger \Phi - \frac{v^2}{2} \right]^n \right\} \quad (5.13)$$

Compared to the form we have given in 1.1, the first term in this series ($n = 2$) normalised with $\kappa_2 = a_2 = 1$, is the usual minimal \mathcal{SM} potential; whereas for $n > 2$, $\kappa_n = g^{2(n-2)} \frac{a_n}{(n-1)^2}$. Because of the new scale, this expansion suggests a hierarchy such that the dominant term (besides the \mathcal{SM} contribution) would correspond to $n = 3$. Truncating the expansion at this order, the leading parts of the potential that contribute to the processes we have been studying write:

$$V_{SSB} = \frac{1}{2} M_H^2 \left\{ H^2 + \frac{g}{M_W} H(\varphi^+ \varphi^- + \frac{\varphi_3^2}{2}) + \frac{g}{2M_W} h_3 H^3 \right. \\ \left. h_4 \left(\frac{g}{4M_W} \right)^2 H^4 + h'_3 \left(\frac{g}{2M_W} \right)^2 H^2(\varphi^+ \varphi^- + \frac{\varphi_3^2}{2}) \dots \right\} \quad (5.14)$$

Note that the $H\varphi^+\varphi^-$ is unaffected, while not only the strength parameterising the H^3 coupling, h_3 , but also the quartic h_4 (H^4) as well as $H^2\varphi^+\varphi^-$ get a contribution at this order, such that their resulting strengths are not in the same ratio as in the \mathcal{SM} .

$$\begin{aligned} h_3 &= 1 + a_3 \frac{M_W^2}{\Lambda^2} = 1 + \delta h_3 \\ h_4 &= 1 + 6\delta h_3 \\ h'_3 &= 1 + 3\delta h_3 \end{aligned} \quad (5.15)$$

It is worth observing that had we done the calculation for $\gamma\gamma \rightarrow W^+W^-HH$ with the usual linear gauge fixing condition in a renormalisable gauge we would have had to add

an anomalous $H^2\varphi^+\varphi^-$ contribution. No such addition is needed with the gauge fixing we have exploited.

There is yet another gauge invariant implementation of the triple Higgs vertex, that also maintains the custodial SU(2) symmetry. Symmetry breaking can be realised non-linearly as one would be led to assume in the limit of a very heavy (or no) Higgs scenario. In this picture the Higgs would have to be interpreted as a scalar that has to be coupled in a chirally invariant way to the Goldstones. The latter may be collected in the matrix Σ with

$$\Sigma = \exp\left(\frac{i\omega^i\tau^i}{v}\right) \quad \mathcal{D}_\mu\Sigma = \partial_\mu\Sigma + \frac{i}{2}(g\mathbf{W}_\mu\Sigma - g'B_\mu\Sigma\tau_3) \quad (5.16)$$

The most general lowest order Lagrangian that represents the symmetry breaking sector is[25]

$$\begin{aligned} \mathcal{L}_{SSB}^{(2)} &= \frac{1}{4}(v^2 + 2h_1vH + h_2H^2 + \dots) \text{Tr}(\mathcal{D}^\mu\Sigma^\dagger\mathcal{D}_\mu\Sigma) + \frac{1}{2}(\partial_\mu H)^2 \\ &- \frac{1}{2}M_H^2\left(H^2 + \frac{g}{2M_W}h_3H^3 + h_4\left(\frac{g}{4M_W}\right)^2 H^4 + \dots\right) \end{aligned} \quad (5.17)$$

In the standard model all $h_i = 1$. $h_{1,2}$ represent $VVH, VVHH$ interactions which in our study we took to be standard. h_1 can be probed in other reactions (such as Higgs decays or single Higgs production) where h_3 does not take part. taking only $h_3 \neq 1$ would be unnatural.

5.2 Identifying the triple Higgs vertex in double Higgs production

Beside the fact that the cross sections for double Higgs production are quite small, the extraction of the h_3 part is not so easy. We have seen that already at the level of $WW \rightarrow HH$ the cross section is dominated by forward/backward events and the effect of H^3 is blurred. There is though a specific signature of the H^3 coupling in all processes that we have studied. Once we note that the two Higgses that originate from this vertex can be regarded as produced by a scalar H^* then in the centre of mass system of the pair, the angular distribution of the Higgses is flat. Therefore, we suggest to reconstruct the angle, θ^* , measured in the centre-of-mass of the pair, between the Higgs direction and the boost axis (or for that matter the reference direction Oz of the beam). For the signal events the distribution is flat, while the background events are peaked in the forward/backward

direction. In Figs. 23 we show, for $\gamma\gamma \rightarrow W^+W^-HH$, the distributions in this variable for the signal as well as the background and the interference terms, that clearly make and confirms the point: The signal does not show any dependence on the angle θ^* , while the “background” is clearly peaked in the forward direction and the interference shows some angular dependence.

For $e^+e^- \rightarrow \nu_e\bar{\nu}_eHH$ boosting back one obviously obtains the same angular distribution as for $W^+W^- \rightarrow HH$. It is clear that to improve the detection of the H^3 or get a better limit on its self-coupling one should keep to the central region in θ^* . One possibility is to consider the ratio of events within a central region, characterised by an optimised angle θ_0^* , over the number of events outside this region:

$$R = \frac{\sigma_{HH}(|\cos\theta^*| < |\cos\theta_0^*|)}{\sigma_{HH}(|\cos\theta^*| > |\cos\theta_0^*|)} \quad (5.18)$$

As with almost all ratios, this has the advantage of being free of many of the uncertainties in measuring the cross section as well as some of the theoretical uncertainties. Here we have in mind the choice of the input parameters which for a 6-particle amplitude in the electroweak theory can introduce large uncertainties as we pointed out in section 2.

5.3 Measuring h_3 in $e^+e^- \rightarrow \nu_e\bar{\nu}_eHH$

For the $e^+e^- \rightarrow \nu_e\bar{\nu}_eHH$, the h_3 coupling appears in only one of the diagrams. We have also looked at whether the W_L approximation works when we include a non-standard coupling. The answer is that the approximation is as good as with what we found for the \mathcal{SM} . That is, at 100GeV the approximation is not to be trusted since it overestimates the cross section by a factor of 2, while for 400GeV the approximation is excellent, see Fig. 24. For the measurements of the coupling we concentrated essentially on the 2TeV collider. We will content ourselves with a brief comment about what would happen with a higher energy “futuristic” machine.

We assume that, at $\sqrt{s} = 2TeV$ one will be able to collect a total integrated luminosity of $300fb^{-1}$. Moreover, we assume an efficiency for the reconstruction of the double Higgs events to be 50%. We will be conservative in the sense that we base our results as if no initial polarisation were available, remembering that if beam polarisation were available one could gain a factor of four in statistics.

At 2TeV this leads to an event sample of ~ 68 HH events for $M_H = 100GeV$ whose signature is $4b$ events plus large missing energy. One obvious background is $\nu\nu ZZ$, but we assume that invariant mass constraints should get rid of these as they should for $WW\nu\bar{\nu}$

Figure 23: *The distribution in the reconstructed angle θ^* for the signal, background and the interference in the case of $\gamma\gamma \rightarrow W^+W^-HH$ without convolution with photon spectra.*

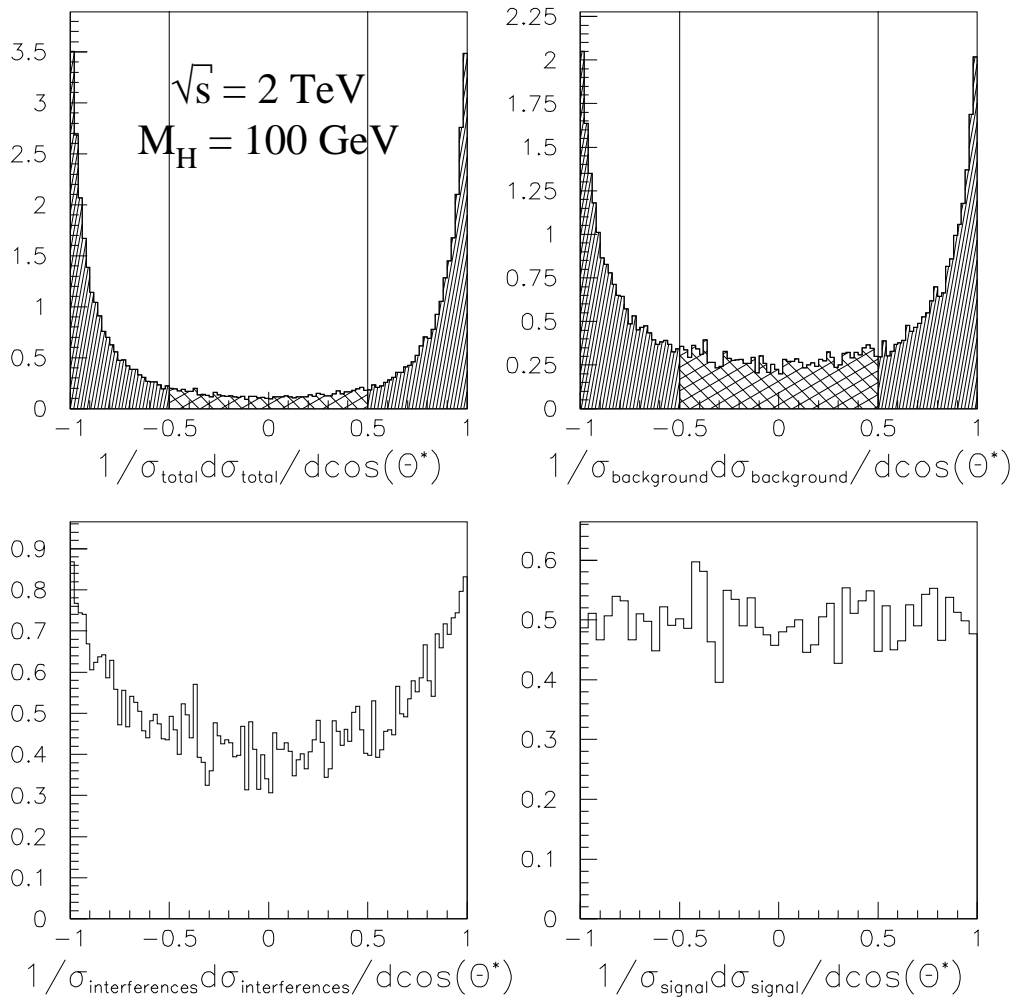
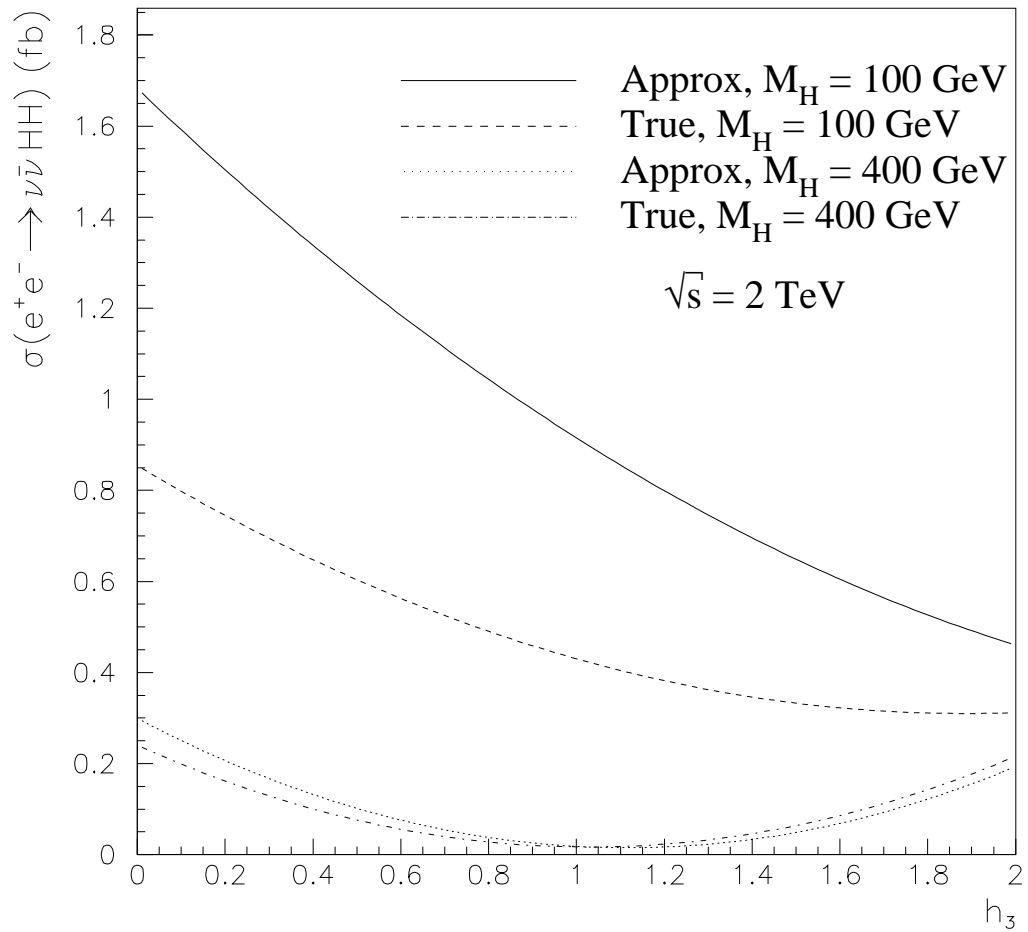


Figure 24: Dependence of the $e^+e^- \rightarrow \nu_e\bar{\nu}_e HH$ cross section on the self-coupling h_3 at 2TeV for $M_H = 100, 400\text{GeV}$. Both the exact calculation and the effective W_L are shown.



if no b tag were available. Of course, for a Higgs with a mass closer to M_Z the situation would be problematic if not hopeless. Considering this not so high statistics we further *conservatively* take as a criterion for detection of an anomaly in h_3 that one has a 50% deviation in the expected number of events, provided one has at least 30 events. With this setting, we conclude from Fig. 24 that with the total cross section one would only be able to claim New Physics if $\delta h_3 < -0.75$ (for positive δh_3 one needs values in excess of $\simeq 2$). For $M_H = 400\text{GeV}$, SM values will not lead to a measurement (in this case the signal is $4W$ plus large missing energy), however if $|\delta h_3| > 1$ a signal will be recorded (there will “unexpectedly be more than 30 events”) and would be a clear indication for an anomalous h_3 coupling.

For $M_H = 100\text{GeV}$ where one has enough events for a \mathcal{SM} value, the ratio R that we introduced earlier is much more powerful in constraining the coupling. For θ^* we took $|\cos\theta^*| < 0.5$. We have not made any effort to optimise this value. First the event sample (with the luminosity and efficiency taken above) within $|\cos\theta^*| < 0.5$ is about 7 out of 60 outside this region. Assuming that the ratio can be measured at 20%, we find $-.10 < |\delta h_3| < .15$ (see Fig. 25) which means a precision of about 10% on h_3 .

Let us comment briefly about how much better a higher energy e^+e^- machine can do. To see this we refer to Fig. 16 that shows, at 5TeV , the Higgs mass dependence of the cross section for both the signal and the background. We can conclude that for $M_H = 700\text{GeV}$ switching off the triple Higgs vertex ($h_3 = 0$, that corresponds to taking into account only the “Backgrounds diagrams”) leads to a 10 fold increase of the cross section!

5.4 Measuring h_3 in $\gamma\gamma \rightarrow W^+W^-HH$

From the detailed analysis on the $\gamma\gamma \rightarrow W^+W^-HH$ process, we learnt that at 2TeV the cross section is lower than in $e^+e^- \rightarrow \nu_e\bar{\nu}_eHH$ and this even before taking into account the reduction introduced by the convolution and the branching ratios of the W ’s (if not all W decays are used for the analysis). Of course, at much higher energies and with higher masses the $\gamma\gamma$ mode fares better. In any case, as concerns the triple Higgs vertex one advantage of the $\gamma\gamma$ mode is that this coupling takes part not only in the fusion diagrams but also in the bremsstrahlung type diagrams which are not negligible at 2TeV , especially for a light Higgs. Taking the effective $\gamma\gamma$ luminosity to be only half that of the e^+e^- and with the same efficiency for reconstruction of double Higgs events, for $M_H = 100\text{GeV}$, one can hope to collect 15 events. In view of this number our criterion for detection of

Figure 25: Dependence of the ratio R on h_3 both for $\gamma\gamma \rightarrow W^+W^-HH$ and $e^+e^- \rightarrow \nu_e\bar{\nu}_eHH$.

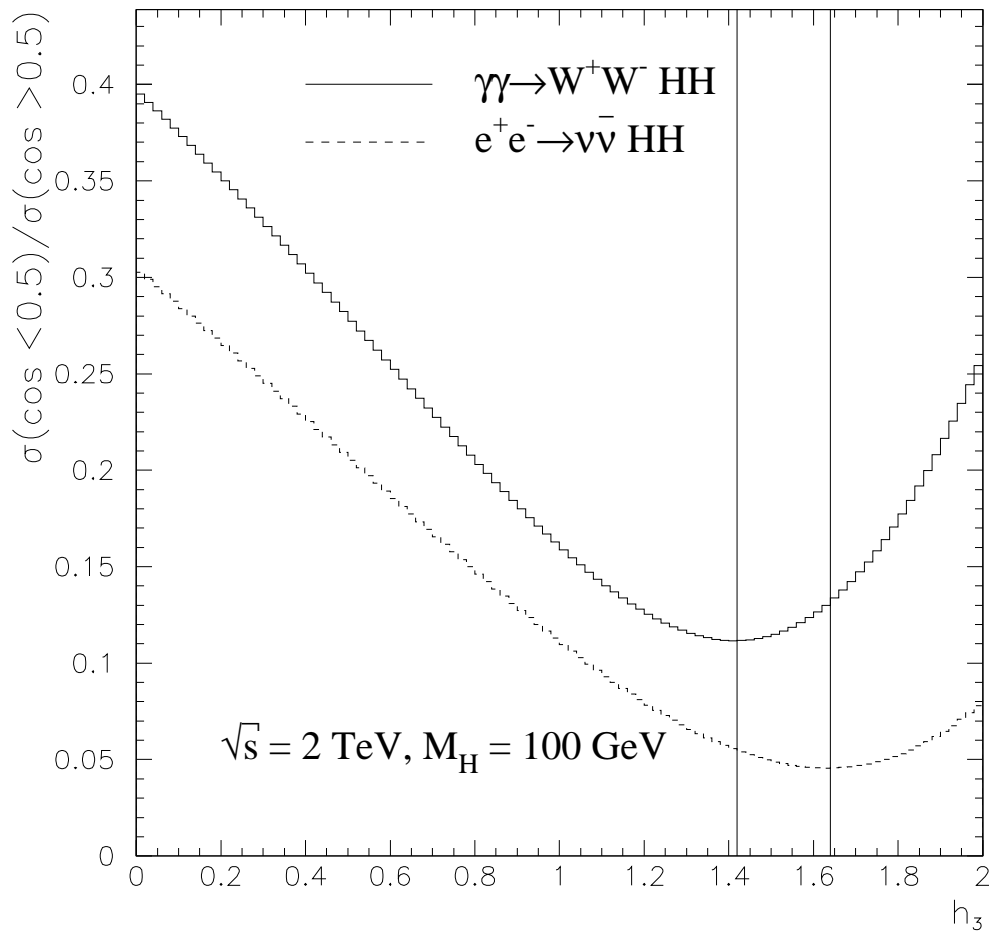
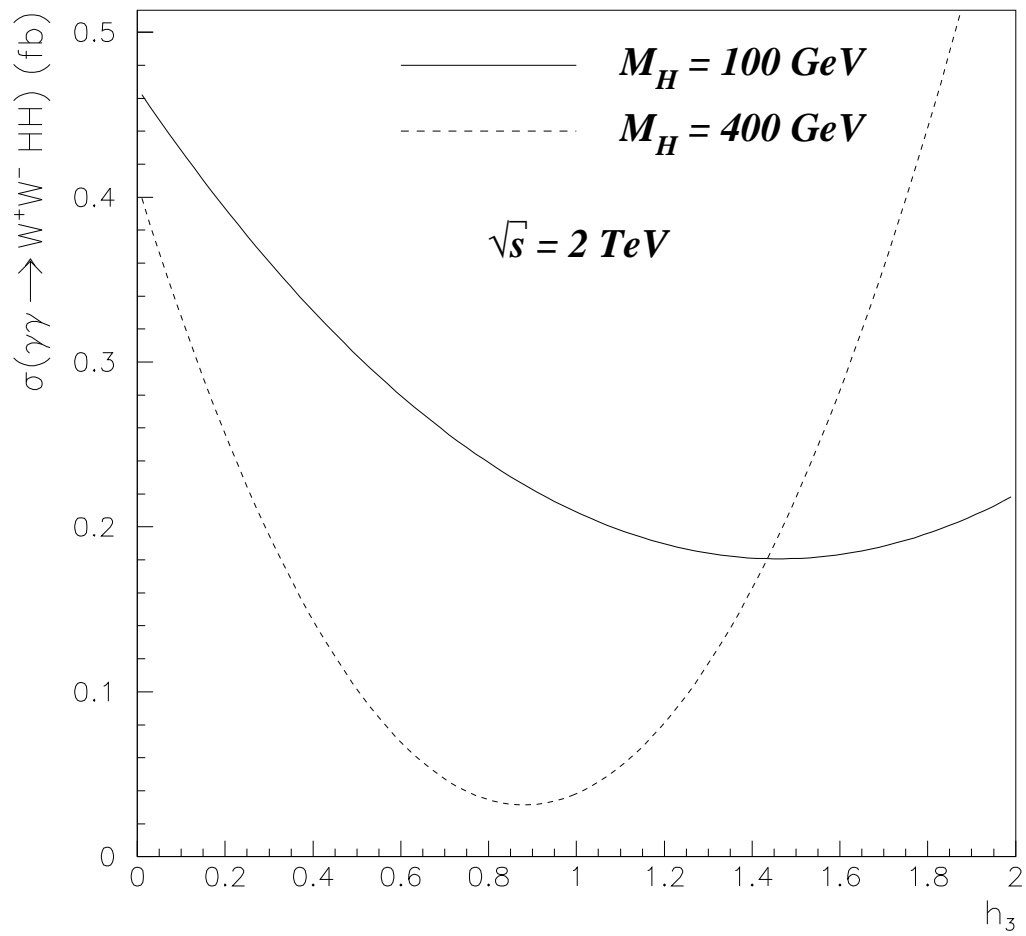


Figure 26: Dependence of the $\gamma\gamma \rightarrow W^+W^-HH$ cross section on the self-coupling h_3 at 2TeV for $M_H = 100, 400\text{GeV}$.



non-standard values is 100% deviation in the number of events which, here means that we require a doubling of events. In this case there is a very slight improvement on the limit extracted from the total $e^+e^- \rightarrow \nu_e\bar{\nu}_e HH$ cross: $\delta h_3 < -0.5$ which in any case does not compete with the limit one extracts from the ratio R in e^+e^- . However, we find that for a Higgs mass of 400GeV the effect of an anomalous H^3 coupling are dramatic and, by far, much more interesting than in e^+e^- . Requiring observation of at least 15 events for $M_H = 400\text{GeV}$ (where within the \mathcal{SM} one expects only about 3) useful constraint on the coupling can be set: $-.7 < \delta h_3 < 0.5$. There is thus a complementarity between the e^+e^- and the $\gamma\gamma$ depending on the Higgs mass in probing the Higgs triple vertex even at 2TeV. As for the ratio R , taking $M_H = 100\text{GeV}$ it is unlikely that with the number of total $WWHH$ events at $\gamma\gamma$ one would be able to make such a measurement, nonetheless even if this ratio were measured with the same precision as in e^+e^- one would not constrain the couplings further than what is achieved in the classic e^+e^- mode.

The limits on h_3 we have extracted for a light Higgs from a measurement of R in e^+e^- and the ones for heavy Higgs up to a mass around 400GeV are much better than what could be achieved with the reaction $\gamma\gamma \rightarrow HH$ which is dominated by a $J_Z = 2$ contribution that is insensitive to the the $J_Z = 0$ s-channel Higgs exchange. However, with $\sqrt{s} = 2\text{TeV}$, for $M_H > 600\text{GeV}$ $\gamma\gamma \rightarrow HH$ is the only reaction where useful limits, of the order of what we extracted for lower Higgs in $e^+e^- \rightarrow \nu_e\bar{\nu}_e HH$ and $\gamma\gamma \rightarrow W^+W^-HH$, can be set. Thus, there is at a 2TeV collider a very nice coverage of the h_3 sensitivity by all three reactions. Of course, as the energy increases and especially if the Higgs mass is large, $\gamma\gamma \rightarrow W^+W^-HH$ is the ideal laboratory for testing the h_3 coupling, provided there is enough luminosity in the $\gamma\gamma$ mode and other “technical” problems for the would-be novel colliders are under control.

One may wonder whether it is at all possible to extract an indirect limit on h_3 from low-energy experiments. This is difficult since present data are not very sensitive to even the Higgs mass, let alone to its tri-linear coupling. The latter would only enter at two-loop for current observables **. Considering that we would be dealing with a non renormalisable theory if the Higgs coupling is anomalous, an unambiguous limit is not possible. Only an expected order of magnitude can be given based on “naturalness argument” [26]. This is like trying to constrain the anomalous weak vector bosons couplings from radiative corrections compared to a direct limit through W pair production. The indirect limit on h_3 has been investigated in [4] by considering the effect of h_3 on the ρ parameter. Even

**At one-loop, it only enters for the renormalisation of the Higgs mass.

with the proviso that the estimate from the two-loop calculation is only an indication on the order of magnitude, the indirect limit is an order of magnitude worse than the direct limits covered by the three main double Higgs cross section at 2TeV.

6 Conclusions

The investigation of the scalar potential or the nature of the Higgs, as revealed through its self-couplings, can be done most unambiguously through double Higgs production. For the planned colliders in the foreseeable future the expected cross sections are rather small thus the need to study these signatures in an environment with the least and best understood backgrounds. We have seen that e^+e^- colliders operating at 2TeV centre-of-mass offer great possibilities especially if use is made to run them in both the usual e^+e^- mode as well as the $\gamma\gamma$ mode. We have found that with the realistic luminosities expected for these machines one may hope to achieve a measurement of the tri-linear couplings at the level of 10% (for a light Higgs). The results are also encouraging in the sense that the e^+e^- and the $\gamma\gamma$ modes can cover different ranges of the Higgs mass if a 2TeV machine is built. We find that for a light Higgs (up to 250GeV) the best limits on the H^3 couplings come from $e^+e^- \rightarrow \nu_e\bar{\nu}_e HH$. However, for heavier Higgses up to mass of 500GeV, the best channel is the associated double Higgs production in $\gamma\gamma$. For still heavier masses, the one-loop induced $\gamma\gamma \rightarrow HH$ is by far better, mainly because of its larger phase space. We have proposed the variable R that clearly helps in discriminating the triple Higgs vertex. As a by-product we have verified the validity of the distribution function describing the longitudinal W content of the photon. We find, as with the case of single H production[17], that for a heavy Higgs ($M_H > 400GeV$) the approximation works quite well, although not as well as for the electrons. This is due to the bremsstrahlung contributions that accompany $\gamma\gamma$ production modes and which are often absent in the e^+e^- mode. Another critical issue that our study has addressed and which comes as a by-product of our results, is how much better a $\gamma\gamma$ collider fares in probing models of strongly interacting W 's that would have to manifest themselves in the absence of a light Higgs. The answer is directly related to the luminosity of $W_L W_L$ that one effectively gets at the two modes.

Translating our comparisons for the heavy Higgs production and combining them with our previous findings about single heavy Higgs production[12], the conclusion is that we can indeed arrive at a higher luminosity in the $\gamma\gamma$ mode. However, when we include realistic photon spectra the factor two enhancement provided in the $\gamma\gamma$ mode is lost in the

convolution, especially if we take into account the new results on the spectra that simulate multiple scattering and include non-linear QED effects[23]. Moreover, this factor 2 can easily go in favour of the e^+e^- mode if both the electron and the positron are polarised. Nonetheless, the e^+e^- mode will only be open to the $W_L^+W_L^-$ channel, while $\gamma\gamma$ provides all combinations of charges.

Another result of our study concerns the computational part. We have advocated the use of non-linear gauge fixing conditions[6] for *tree-level* multiple bosons processes in $\gamma\gamma$ reactions and have made the connection with the background field gauge-fixing constraints. These types of gauges tremendously ease the calculational task. We foresee their use for all calculations in the framework of the laser induced high-energy $\gamma\gamma$ collider.

Note added

During the writing up of this paper, there appeared[27] a new “automatic” calculation of $\gamma\gamma \rightarrow W^+W^-HH$ in the unitary gauge. Our results agree with the ones found in[27] when we take the same input parameters. Note, however, that most of the results of this paper have been presented at the *2nd European Workshop on Physics with e^+e^- Colliders*[28] and in[29] prior to [27].

Acknowledgements

It is with great pleasure that we wish to thank Geneviève Bélanger and Marc Baillargeon for their ever unfailing help and comments. We are also very grateful to George Jikia for the many discussions and for most kindly providing us with his program for $\gamma\gamma \rightarrow HH$. One of us (E.C) thanks Xavier Artru for interesting discussions about multiperipheral processes.

A Appendix: Feynman Rules for the Generalised Non-Linear Gauge Fixing Condition

We begin by presenting our conventions and notations for the bosonic sector of the $SU(2) \times U(1)$ model.

The $SU(2)$ gauge fields are $\mathbf{W}_\mu = W_\mu^i \tau^i$, while the hypercharge field is denoted by $\mathbf{B}_\mu = \tau_3 B_\mu$. The normalisation for the Pauli matrices is $\text{Tr}(\tau^i \tau^j) = 2\delta^{ij}$. The radiation

Lagrangian is expressed *via* field strength, $\mathbf{W}_{\mu\nu}$

$$\begin{aligned}\mathbf{W}_{\mu\nu} &= \frac{1}{2} \left(\partial_\mu \mathbf{W}_\nu - \partial_\nu \mathbf{W}_\mu + \frac{i}{2} g [\mathbf{W}_\mu, \mathbf{W}_\nu] \right) \\ &= \frac{\tau^i}{2} \left(\partial_\mu W_\nu^i - \partial_\nu W_\mu^i - g \epsilon^{ijk} W_\mu^j W_\nu^k \right)\end{aligned}\tag{A.1}$$

and

$$\mathbf{B}_{\mu\nu} = \frac{1}{2} (\partial_\mu B_\nu - \partial_\nu B_\mu) \tau_3\tag{A.2}$$

such that the pure gauge kinetic term writes

$$\mathcal{L}_{\text{Gauge}} = -\frac{1}{2} [\text{Tr}(\mathbf{W}_{\mu\nu} \mathbf{W}^{\mu\nu}) + \text{Tr}(\mathbf{B}_{\mu\nu} \mathbf{B}^{\mu\nu})]\tag{A.3}$$

The Higgs doublet, Φ , with hypercharge $Y = 1$, is written as

$$\begin{pmatrix} \varphi^+ \\ \frac{1}{\sqrt{2}}(v + H + i\varphi_3) \end{pmatrix}$$

and the covariant derivative acting on this doublet is such that

$$\mathcal{D}_\mu \Phi = \left(\partial_\mu + \frac{i}{2} (g \mathbf{W}_\mu + g' Y B_\mu) \right) \Phi\tag{A.4}$$

The Higgs potential is introduced

$$\mathcal{V}_{SSB} = \lambda \left[\Phi^\dagger \Phi - \frac{\mu^2}{2\lambda} \right]^2\tag{A.5}$$

with $\mu^2, \lambda > 0$ such that spontaneous symmetry breaking ensues. The W^\pm and Higgs masses are

$$M_W = \frac{gv}{2} \quad M_H^2 = 2\mu^2 = 2\lambda v^2 \quad v = 246 \text{ GeV}\tag{A.6}$$

Our convention for the fields and couplings is

$$Z_\mu = c_W W_\mu^{(3)} - s_W B_\mu\tag{A.7}$$

$$A_\mu = s_W W_\mu^{(3)} + c_W B_\mu\tag{A.8}$$

$$g = e/s_W\tag{A.9}$$

$$g' = e/c_W\tag{A.10}$$

$$g_Z = e/s_W c_W\tag{A.11}$$

We propose, when one is dealing with multiparticle final states that involve photons and weak bosons, to use the generalised non-linear gauge fixing condition, both for the W

$$\mathcal{L}_{\xi_W} = -\frac{1}{\xi_W} |(\partial_\mu + ie\tilde{\alpha}A_\mu + ig\cos_W\tilde{\beta}Z_\mu)W^{\mu+} + i\xi_W\frac{g}{2}(v + \tilde{\delta}H - i\tilde{\kappa}\varphi_3)\varphi^+|^2 \quad (\text{A.12})$$

and Z

$$\mathcal{L}_{\xi_Z} = -\frac{1}{2\xi_Z} (\partial \cdot Z + \xi_Z \frac{g}{2\cos_W} (v + \tilde{\varepsilon}H)\varphi_3)^2 \quad (\text{A.13})$$

The most practical choice for the ξ_i is $\xi_W = \xi_Z = \xi = 1$. We do not touch the gauge fixing for the photon:

$$\mathcal{L}_\xi = -\frac{1}{2\xi} (\partial \cdot A)^2 \quad (\text{A.14})$$

As we pointed earlier these gauge fixing conditions have to be paralleled with the gauge fixing constraints one imposes in the background-field method. In the latter, upon splitting the fields ψ into into their classical, ψ_{cl} , and quantum, ψ_Q , parts: $\psi = \psi_{cl} + \psi_Q$ and specialising to the case where the gauge parameters ξ are all equal, one has for the $SU(2) \times U(1)$ theory (see for instance[9])

$$\begin{aligned} \mathcal{L}^{bckgrd} &= -\frac{1}{\xi} |(\partial \cdot W_Q^+ + ig(W_{cl}^{(3)} \cdot W_Q^+ - W_Q^{(3)} \cdot W_{cl}^+) + \frac{i}{2}\xi S^+|^2 \\ &- \frac{1}{2\xi} |(\partial \cdot A_Q + ie(W_{cl}^+ \cdot W_Q^- - W_Q^+ \cdot W_{cl}^-) + ie\xi(\varphi_Q^+ \varphi_{cl}^- - \varphi_{cl}^+ \varphi_Q^-))|^2 \\ &- \frac{1}{2\xi} |(\partial \cdot Z_Q + igc_W(W_{cl}^+ \cdot W_Q^- - W_Q^+ \cdot W_{cl}^-) \\ &+ i\xi \frac{1}{2s_W c_W} ((c_W^2 - s_W^2)(\varphi_Q^+ \varphi_{cl}^- - \varphi_{cl}^+ \varphi_Q^-) + i(H_Q \varphi_{3cl} - (v + H_{cl})\varphi_{3Q}))|^2 \\ S^+ &= \varphi_Q^+(v + H_{cl} - i\varphi_{3cl}) - \varphi_{cl}^+(H_Q - i\varphi_{3Q}) \end{aligned} \quad (\text{A.15})$$

The identification with the non-linear gauge-fixing constraint is the following. For the $\gamma\gamma$ processes we have been studying, one does not need a gauge-fixing for the photon (and the Z). These are then considered purely classical as is the corresponding neutral Goldstone and the Higgs. On the other hand, since there is no separation, in the non-linear gauge, between classical and quantum fields one interprets the W^\pm and their Goldstones

as “quantum”. Then making $W_{cl}^\pm, \varphi_{cl}^\pm \rightarrow 0$ (but $W_Q^{(3)}, H_Q \rightarrow 0$) leads to the charged part of the non-linear gauge constraint with

$$\tilde{\alpha} = \tilde{\beta} = \tilde{\delta} = \tilde{\kappa} = 1 \quad (\text{A.16})$$

Which are the values that bring the most simplifications in practical calculations. Note, however that if we *also* fix the gauge in the neutral sector then the identification is less transparent, as mixtures necessarily occur. In A.13, for instance, and with $\tilde{\varepsilon} = 1$, H is to be interpreted classical whereas φ_3 is necessarily quantum like the Z .

This is the gauge we have taken in this paper (although we did not need to specify $\tilde{\varepsilon}$).

At this point it is worth comparing with specific examples of non-linear gauges that have been used for loop calculations. The condition used in[6] can be recovered by setting

$$\tilde{\alpha} = \tilde{\beta} = 1 \quad \tilde{\delta} = \tilde{\kappa} = \tilde{\varepsilon} = 0 \quad (\text{A.17})$$

This condition gets rid of $W^\pm \varphi^\mp \gamma$ and has the advantage of keeping the same Lorentz structure for the tri-linear $WW\gamma$ and WWZ vertices. However, the vertices $W^\pm \varphi^\mp Z$ and $W^\pm \varphi^\mp H(A, Z)$ are present. The condition taken in[19] corresponds to

$$\tilde{\alpha} = \tilde{\delta} = \tilde{\varepsilon} = 1 \quad \tilde{\beta} = \tilde{\kappa} = 0 \quad (\text{A.18})$$

Here both $W^\pm \varphi^\mp \gamma$ and $W^\pm \varphi^\mp HA$ vanish.

In[30] both $W^\pm \varphi^\mp \gamma$ and $W^\pm \varphi^\mp Z$ are made to vanish. One can see that this is arrived at by taking $\tilde{\alpha} = 1, \tilde{\delta} = \tilde{\varepsilon} = \tilde{\kappa} = 0$, while

$$\tilde{\beta} = -\frac{s_W^2}{c_W^2} \quad (\text{A.19})$$

This corresponds to a $U(1)_Y$ covariant derivative. However, contrary to what is claimed in [30], with this choice, $W^\pm \varphi^\mp H(Z, \gamma)$ still remain (but luckily these vertices have no incidence on the calculation $\gamma\gamma \rightarrow ZZ$ in[30]).

We now give the Feynman rules for the generalised non-linear gauge fixing condition:

Propagators

$$\Pi_{\mu\nu}^W = \frac{-i}{k^2 - M_W^2} \left[g_{\mu\nu} + \frac{(\xi_W - 1)k_\mu k_\nu}{k^2 - \xi_W M_W^2} \right] \quad (\text{A.20})$$

$$\Pi_{\mu\nu}^Z = \frac{-i}{k^2 - M_Z^2} \left[g_{\mu\nu} + \frac{(\xi_Z - 1)k_\mu k_\nu}{k^2 - \xi_Z M_Z^2} \right] \quad (\text{A.21})$$

$$\Pi_{\mu\nu}^{\gamma} = \frac{-i}{k^2} \left[g_{\mu\nu} + \frac{(\xi_{\gamma} - 1)k_{\mu}k_{\nu}}{k^2} \right] \quad (\text{A.22})$$

$$\Pi^H = \frac{i}{k^2 - m_H^2} \quad (\text{A.23})$$

$$\Pi^{\varphi_3} = \frac{i}{k^2 - \xi_Z M_Z^2} \quad (\text{A.24})$$

$$\Pi^{\varphi^{\pm}} = \frac{i}{k^2 - \xi_W M_W^2} \quad (\text{A.25})$$

$$\Pi^{\eta_{\gamma}} = \frac{i\xi_{\gamma}}{k^2} \quad (\text{A.26})$$

$$\Pi^{\eta_Z} = \frac{i\xi_Z}{k^2 - \xi_Z M_Z^2} \quad (\text{A.27})$$

$$\Pi^{\eta^{\pm}} = \frac{i\xi_W}{k^2 - \xi_W M_W^2} \quad (\text{A.28})$$

As is obvious, for all calculations $\xi_i = 1$ is to be preferred.

Trilinear vertices

In the following all momenta are taken to be incoming.

$$\begin{array}{c}
 W^{+\alpha}(p_+) \\
 \left. \begin{array}{l} \text{---} \\ \text{---} \\ \text{---} \end{array} \right\} \\
 [\gamma^{\mu}; Z^{\mu}](k) \\
 \left. \begin{array}{l} \text{---} \\ \text{---} \end{array} \right\} \\
 W^{-\beta}(p_-)
 \end{array}
 \quad -ie \left[1; \frac{c_W}{s_W} \right] \left[g_{\alpha\beta}(p_- - p_+)_{\mu} + \left(1 + \frac{\tilde{\alpha}}{\xi_W} \right) (k_{\alpha}g_{\mu\beta} - k_{\beta}g_{\mu\alpha}) \right. \\
 \left. + \left(1 - \frac{\tilde{\alpha}}{\xi_W} \right) (g_{\mu\alpha}p_{+\beta} - g_{\mu\beta}p_{-\alpha}); \tilde{\alpha} \rightarrow \tilde{\beta} \right]$$

The form of this vertex calls for some comments. First, when $\tilde{\alpha}$ and $\tilde{\beta}$ are equal the vertices have, apart from an overall constant, the same Lorentz structure. The first term, that does not depend on any of the gauge-fixing parameters, corresponds to the convection current. This is the same current that one obtains for scalars and indeed, apart from the $g_{\alpha\beta}$ term that counts the vector degrees of freedom, this is exactly as in scalar electrodynamics. When we further take the most “practical values” $\tilde{\alpha} = \tilde{\beta} = 1$ (that correspond to taking a covariant derivative along the T_3 direction) and with $\xi_W = 1$ the third term vanishes and the second is nothing else but the spin current with the correct value for the magnetic moment of a spin-1 gauge particle.

$$\begin{array}{c}
W^{\pm\nu}(p_W) \\
\text{---} \text{---} \text{---} \\
[\gamma^\mu; Z^\mu] \text{---} \text{---} \text{---} \\
\text{---} \text{---} \text{---} \\
\varphi^\mp(p_\varphi)
\end{array}
\quad ig^{\mu\nu}[eM_W(1 - \tilde{\alpha}); -gM_Z(1 - c_W^2(1 - \tilde{\beta}))]$$

One can make both the $W^\pm\varphi^\mp Z$ and $W^\pm\varphi^\mp\gamma$ vanish. While the vanishing of the photon part is for the value $\alpha = 1$ that makes the $WW\gamma$ (and as we will see the $WW\gamma\gamma$) simple, the vanishing of the $W^\pm\varphi^\mp Z$ requires $\tilde{\beta} = -s_W^2/c_W^2$ that does not make the other vertices simpler. Note that these vertices do not depend on ξ_W . The remaining tri-linear vertices that we list below can not be made to vanish.

$$\begin{array}{c}
[W^{+\rho}(p_+); Z^\rho] \\
\text{---} \text{---} \text{---} \\
H \text{---} \text{---} \text{---} \\
\text{---} \text{---} \text{---} \\
[W^{-\sigma}(p_-); Z^\sigma]
\end{array}
\quad ig^{\rho\sigma}[gM_W; g_Z M_Z]$$

$$\begin{array}{c}
W^{\pm\mu}(p_W) \\
\text{---} \text{---} \text{---} \\
H \text{---} \text{---} \text{---} \\
\text{---} \text{---} \text{---} \\
\varphi^\mp(p_\varphi)
\end{array}
\quad \pm i \frac{g}{2} ((1 - \tilde{\delta})p_\varphi - (1 + \tilde{\delta})p_H)^\mu$$

$$\begin{array}{c}
W^{\pm\mu}(p_W) \\
\text{---} \text{---} \text{---} \\
\varphi_3 \text{---} \text{---} \text{---} \\
\text{---} \text{---} \text{---} \\
\varphi^\mp(p_\varphi)
\end{array}
\quad -\frac{g}{2} ((1 - \tilde{\kappa})p_\varphi - (1 + \tilde{\kappa})p_{\varphi_3})^\mu$$

$$\begin{array}{c}
\varphi^+(p_+) \\
\text{---} \text{---} \text{---} \\
[\gamma^\mu; Z^\mu] \text{---} \text{---} \text{---} \\
\text{---} \text{---} \text{---} \\
\varphi^-(p_-)
\end{array}
\quad -i \left[e; g_Z \frac{c_W^2 - s_W^2}{2} \right] (p_+ - p_-)^\mu$$

$$\begin{array}{c}
Z^\mu \\
\text{---} \\
\text{---} \\
\varphi_3
\end{array}
\frac{g_Z}{2} ((1 + \tilde{\varepsilon})p_H - (1 - \tilde{\varepsilon})p_{\varphi_3})^\mu$$

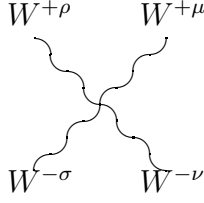
$$\begin{array}{c}
H \\
\text{---} \\
\text{---} \\
H
\end{array}
-\frac{3igM_H^2}{2M_W}$$

$$\begin{array}{c}
[\varphi_3; \varphi^+] \\
\text{---} \\
\text{---} \\
[\varphi_3; \varphi^-]
\end{array}
\left[-\frac{ig}{2M_W} (M_H^2 + 2\xi_W \tilde{\delta} M_W^2); (g \rightarrow g_Z, M_W \rightarrow M_Z, \xi_W \rightarrow \xi_Z, \tilde{\delta} \rightarrow \tilde{\varepsilon}) \right]$$

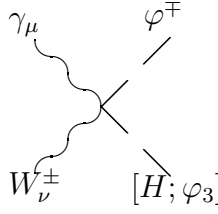
Quartic vertices

$$\begin{array}{c}
W^{+\rho} [\gamma^\mu; \gamma^\mu; Z^\mu] \\
\text{---} \\
\text{---} \\
\text{---} \\
W^{-\sigma} [\gamma^\nu; Z^\nu; Z^\nu]
\end{array}
\begin{array}{l}
-i e^2 [1; c_W/s_W; c_W^2/s_W^2] (2g^{\mu\nu} g^{\rho\sigma} \\
-(g^{\mu\sigma} g^{\nu\rho} + g^{\mu\rho} g^{\nu\sigma}) [(1 - \tilde{\alpha}^2/\xi_W); (1 - \tilde{\alpha}\tilde{\beta}/\xi_W); (1 - \tilde{\beta}^2/\xi_W)])
\end{array}$$

Again for the values that correspond to the T_3 covariant derivative and $\xi_W = 1$ there only remains the same part that one finds for the scalars (apart from the factor counting the vector degrees of freedom).

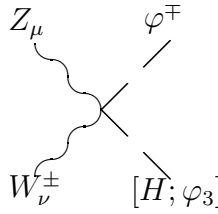


$$ig^2(2g^{\mu\rho}g^{\nu\sigma} - (g^{\mu\sigma}g^{\nu\rho} + g^{\mu\nu}g^{\rho\sigma}))$$



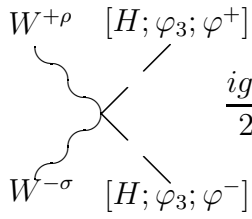
$$[i(1 - \tilde{\alpha}\tilde{\delta}); \mp(1 - \tilde{\alpha}\tilde{\kappa})]\frac{ge}{2}g_{\mu\nu}$$

Note that it is not sufficient to take $\tilde{\alpha} = 1$ to get rid of this vertex.

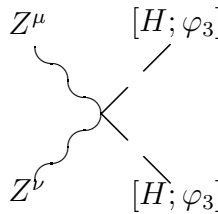


$$[-i(1 - c_W^2(1 - \tilde{\beta}\tilde{\delta})) ; \pm(1 - c_W^2(1 - \tilde{\beta}\tilde{\kappa}))]\frac{gg_Z}{2}g_{\mu\nu}$$

Note that if $\tilde{\delta} = \tilde{\kappa} = 1$ then the same condition that makes the $W^\pm\varphi^\mp Z$ vanish, eliminates this vertex too.



$$\frac{ig^2}{2}g^{\rho\sigma}$$



$$\frac{ig_Z^2}{2}g^{\mu\nu}$$

$$2ie^2 \left[1; \frac{c_W^2 - s_W^2}{2s_W c_W}; \left(\frac{c_W^2 - s_W^2}{2s_W c_W} \right)^2 \right] g^{\mu\nu}$$

$$-i \frac{g^2 M_H^2}{2M_W^2} \left[\frac{3}{2}; \frac{3}{2}; 1 \right]$$

$$-\frac{ig^2}{4M_W^2} (M_H^2 + 2M_Z^2 \tilde{\epsilon}^2 \xi_Z)$$

$$-\frac{ig^2}{4M_W^2} [M_H^2 + 2M_W^2 \tilde{\delta}^2 \xi_W; M_H^2 + 2M_W^2 \tilde{\kappa}^2 \xi_W]$$

Ghosts vertices

Diagram: A wavy line labeled $W^{\pm\mu}$ connects to two ghost lines. The top ghost line is labeled $[\bar{\eta}_\gamma; \bar{\eta}_Z](\bar{p})$ and the bottom ghost line is labeled η_\mp . The vertex factor is $\pm i \bar{p}^\mu [e; g c_W]$.

Diagram: A wavy line labeled $W^{\pm\mu}$ connects to two ghost lines. The top ghost line is labeled $\bar{\eta}_\pm(\bar{p})$ and the bottom ghost line is labeled $[\eta_\gamma; \eta_Z](p)$. The vertex factor is $\mp i [e; g c_W](\bar{p} + [\tilde{\alpha}; \tilde{\beta}]p)^\mu$.

Diagram: A solid line labeled $[H; \varphi^\pm]$ connects to two ghost lines. The top ghost line is labeled $\bar{\eta}_Z$ and the bottom ghost line is labeled $[\eta_Z; \eta_\mp]$. The vertex factor is $-\frac{i m_Z \xi_Z}{2} [g_Z(1 + \tilde{\varepsilon}); -g]$.

Diagram: A solid line labeled φ^\pm connects to two ghost lines. The top ghost line is labeled $\bar{\eta}_\pm$ and the bottom ghost line is labeled $[\eta_\gamma; \eta_Z]$. The vertex factor is $-i M_W \xi_W [e; \frac{g_Z}{2}(\tilde{\kappa} + c_W^2 - s_W^2)]$.

Diagram: A wavy line labeled $[\gamma^\mu; Z^\mu]$ connects to two ghost lines. The top ghost line is labeled $\bar{\eta}_\pm(\bar{p})$ and the bottom ghost line is labeled $\eta_\pm(p)$. The vertex factor is $\pm i [e; g c_W](\bar{p} - [\tilde{\alpha}; \tilde{\beta}]p)^\mu$.

Diagram: A solid line labeled $[H; \varphi_3]$ connects to two ghost lines. The top ghost line is labeled $\bar{\eta}_\pm$ and the bottom ghost line is labeled η_\pm . The vertex factor is $[-i(1 + \tilde{\delta}); \pm(1 - \tilde{\kappa})] \frac{g M_W \xi_W}{2}$.

Diagram: Two solid lines labeled $[H; \varphi_3]$ and two ghost lines labeled $\bar{\eta}_Z$ and η_Z meet at a vertex. The lines cross. The vertex factor is $[-; +] i \xi_Z \tilde{\varepsilon} \frac{g_Z^2}{2}$.

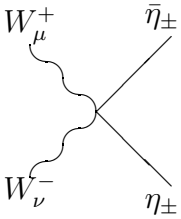
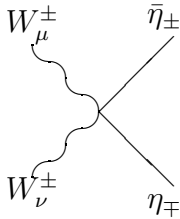
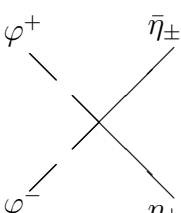
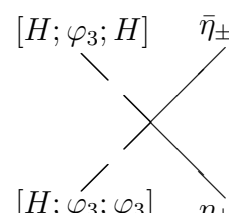
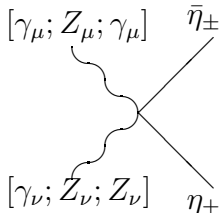
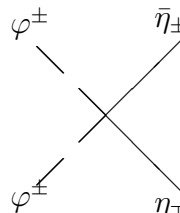
Diagram: Two solid lines labeled $[H; \varphi_3]$ and two ghost lines labeled $\bar{\eta}_Z$ and η_\pm meet at a vertex. The lines cross. The vertex factor is $[i; \mp 1] \tilde{\varepsilon} \xi_Z \frac{g g_Z}{4}$.

Diagram: A wavy line labeled W_μ^\pm and a wavy line labeled $[\gamma_\nu; Z_\nu]$ meet at a vertex. Two ghost lines labeled $\bar{\eta}_\pm$ and η_γ also meet at this vertex. The vertex factor is $-i e g_{\mu\nu} [e \tilde{\alpha}; g c_W \tilde{\beta}]$.

Diagram: A wavy line labeled W_μ^\pm and a wavy line labeled $[\gamma_\nu; Z_\nu]$ meet at a vertex. Two ghost lines labeled $\bar{\eta}_\pm$ and η_Z also meet at this vertex. The vertex factor is $-\frac{i e^2 c_W}{s_W} g_{\mu\nu} [\tilde{\alpha}; \tilde{\beta} \frac{c_W}{s_W}]$.

Diagram: Two solid lines labeled $[H; \varphi_3]$ and two ghost lines labeled $\bar{\eta}_\pm$ and η_γ meet at a vertex. The lines cross. The vertex factor is $-\frac{e^2 \xi_W}{2 s_W} [i \tilde{\delta}; \pm \tilde{\kappa}]$.

Diagram: Two solid lines labeled $[H; \varphi_3]$ and two ghost lines labeled $\bar{\eta}_\pm$ and η_Z meet at a vertex. The lines cross. The vertex factor is $= -\frac{g g_Z \xi_W}{4} [i(\tilde{\kappa} + \tilde{\delta}(c_W^2 - s_W^2)); \pm(\tilde{\delta} + \tilde{\kappa}(c_W^2 - s_W^2))]$.

	$-i(e^2\tilde{\alpha} + g^2c_W^2\tilde{\beta})g_{\mu\nu}$		$2i(e^2\tilde{\alpha} + g^2c_W^2\tilde{\beta})g_{\mu\nu}$
	$i\frac{g^2\xi_W}{4}(\tilde{\delta} + \tilde{\kappa})$		$-\frac{g^2\xi_W}{4}[2i\tilde{\delta}; 2i\tilde{\kappa}; \pm(\tilde{\kappa} - \tilde{\delta})]$
	$i[2e^2\tilde{\alpha}; 2g^2c_W^2\tilde{\beta}; g^2c_Ws_W(\tilde{\alpha} + \tilde{\beta})]g_{\mu\nu}$		$i\frac{g^2\xi_W}{2}(\tilde{\kappa} - \tilde{\delta})$

References

- [1] F. Abe *et al.*, Phys. Rev. Lett. **73** (1994) 225.
- [2] I.F. Ginzburg *et al.*, Nucl. Instrum. Meth. **205** (1983) 47.
I.F. Ginzburg *et al.*, Nucl. Instrum. Meth. **219** (1984) 5.
V.I. Telnov, Nucl. Instrum. Meth. **A294** (1990) 72.
V.I. Telnov, in Proceedings of *Physics and Experiments with Linear Colliders*, p. 739, edited by R. Orava, P. Eerola and M. Nordberg, World Scientific, 1992.
V.I. Telnov, in *Proceedings of the IXth International Workshop on Photon-Photon Collisions.*, p. 369, edited by D.O. Caldwell and H.P. Paar, World Scientific, 1992.
- [3] G. J. Gounaris, D. Schildknecht and F. M. Renard, Phys. Lett. **B83** (1979) 191.
- [4] J. J. vand der Bij, Nucl. Phys. **B267** (1986) 557.
- [5] G.V. Jikia and Yu.F. Pirogov, Phys. Lett. **B283** (1992) 135.
G.V. Jikia, Nucl. Phys. **B412** (1994) 57.

- [6] K. Fujikawa, *Phys. Rev.* **D7** (1973) 393
M. Base and N.D. Hari Dass, *Ann. Phys.* **94** (1975) 349
M.B. Gavela, G. Girardi, C. Malleville and P. Sorba, *Nucl. Phys.* **B193** (1981) 257
N.G. Deshpande and M. Nazerimonfared, *Nucl. Phys.* **B213** (1983) 390
F. Boudjema, *Phys. Lett.* **B187** (1987) 362.
M. Baillargeon and F. Boudjema, *Phys. Lett.* **B272** (1991) 158.
- [7] B. S. de Witt, in *Dynamical Theory of Groups and Fields*, Gordon and Breach, N.Y. 1965.
S. Weinberg, *Phys. Rev.* **D13** (1976) 974.
L.F. Abbott, *Nucl. Phys.* **B185** (1981) 189.
- [8] G. Shore, *Ann. Phys.* **137** (1981) 262.
M. B. Einhorn and J. Wudka, *Phys. Rev.* **D39** (1989) 2758.
- [9] A. Denner, S. Dittmaier, G. Weiglein *Nucl. Phys.* **B440** (1995) 95.
X. Li and Y. Liao, ASITP/94-50 *hep-ph/9409401*.
For a slight variation, see A.G. Morgan and Z. Bern, *Phys. Rev.* **D49** (1994) 6155.
- [10] R.N. Cahn and S. Dawson, *Phys. Lett.* **B136** (1984) 196.
S. Dawson, *Nucl. Phys.* **B249** (1984) 42.
S. Chanowitz and M.K. Gaillard, *Phys. Lett.* **B142** (1984) 196.
G.L. Kane, W.W. Repko and W.B. Rolnick, *Phys. Lett.* **B148** (1984) 367.
J. Lindfors, *Z. Phys.* **C28** (1985) 427.
W.B. Rolnick, *Nucl. Phys.* **B274** (1986) 171.
Z. Kunszt and D.E. Soper, *Nucl. Phys.* **B296** (1988) 253.
- [11] K. Hagiwara, I. Watanabe, P.M. Zerwas, *Phys. Lett.* **B278** (1992) 187.
- [12] M. Baillargeon, G. Bélanger and F. Boudjema, in *Proceedings of Two-Photon Physics from DAΦNE to LEP200 and Beyond*, Paris, 1994, edited by F. Kapusta and J. Parisi (world Scientific, Singapore, 1995), p.267.
- [13] V. Barger, T. Han and R. J. N Phillips, *Phys. Rev.* **D38** (1988) 2766.
- [14] V. Barger, T. Han, *Mod. Phys. Lett.* **A5** (1990) 667.
- [15] K.J.F. Gaemers, F. Hoogeveen, *Z. Phys.* **C26** (1984) 249.
- [16] For a list of references on this process, see G. Bélanger and F. Boudjema, *Phys. Lett.* **B288** (1992) 210.

- [17] M. Baillargeon and F. Boudjema, Phys. Lett. **B317** (1993) 371.
- [18] R.N. Cahn, Nucl. Phys. **B255** (1985) 341.
- [19] G.V. Jikia, *Nucl. Instrum. Methods*, **A335** (1995) 2907; *ibid* IHEP 94-77; *HEP-PH/94-07393*. This process has also been calculated in the unitary gauge by K. Cheung, Phys. Rev. **D50** (1994) 4290.
- [20] For an excellent review, see Z. Bern, Lectures presented at TASI 1992, Boulder, CO. UCLA/93/TEP/5; *hep-ph/9304249*.
- [21] A. Denner, S. Dittmaier and R. Schuster, Bielefeld Preprint, BI-TP 95/04 *HEP/PH-9503442*.
- [22] M. Chanowitz and M. K. Gaillard, Nucl. Phys. **B261** (1985) 379.
B. W. Lee, C. Quigg and H. Thacker, Phys. Rev. **D16** (1977) 1519.
J. M. Cornwall, D. N. Levin and G. Tiktopoulos, Phys. Rev. **D10** (1974) 1145; **D11** (1975) 972 (E).
C. E. Vayonakis, *Nuov. Cim. Lett.* **17** (1976) 383.
- [23] P. Chen, Presented at the $\gamma\gamma$ Workshop, Sheffield, Apr. 7-8 1995.
V. Telnov, Plenary Talk, Photon'95 Conference, Sheffield, G.B., Apr. 8-15 (1995) to appear in the proceedings.
- [24] D. A. Dicus, K. Kallianpur and S. S. D. Willenbrock, Phys. Lett. **B200** (1988) 187.
A. Abbasabadi, W. W. Repko, D. A. Dicus and R. Vega, Phys. Rev. **D38** (1988) 2770.
K. Kallianpur, Phys. Lett. **B215** (1988) 392.
- [25] R. S. Chivukula and V. Koulovassilopoulos, Phys. Lett. **B309** (1993) 371; Phys. Rev. **D50** (1994) 3218.
- [26] A. Manohar and H. Georgi, Nucl. Phys. **B234** (1984) 189.
- [27] V.A. Ilyin et. al, June 1995, KEK CP-030 *hep-ph/9506326*.
- [28] Talk given at the 2nd European Workshop on *Physics with e^+e^- Linear Colliders*, Higgs Session, Assergi, Gran-Sasso, Italy, June 2nd, 1995. See Proceedings.
- [29] E. Chopin, *Tests du secteur scalaire de la théorie électro-faible*, Rapport de Magistère, ENS-Lyon, Septembre 1994.
- [30] D.A. Dicus and C. Kao, Phys. Rev. **D49** (1994) 1265.